Impairment of tight junctions and glucose transport in endothelial cells of human cerebral cavernous malformations

Schneider, H ; Errede, M ; Ulrich, N H ; Virgintino, D ; Frei, K ; Bertalanffy, H

Abstract: Cerebral cavernous malformations (CCMs) often cause hemorrhages that can result in severe clinical manifestations, including hemiparesis and seizures. The underlying mechanisms of the aggressive behavior of CCMs are undetermined to date, but alterations of vascular matrix components may be involved. We compared the localization of the tight junction proteins (TJPs) in 12 CCM specimens and the expression of glucose transporter 1 (GLUT-1), which is sensitive to alterations in TJP levels, in 5 CCM specimens with those in 5 control temporal lobectomy specimens without CCM by immunofluorescence microscopy. The TJPs occludin, claudin-5, and zonula occludens ZO-1 were downregulated at intercellular contact sites and partly redistributed within the surrounding tissue in the CCM samples; there was also a marked reduction of GLUT-1 immunoreactivity compared with that in control specimens. Corresponding analysis using quantitative real-time reverse transcription polymerase chain reaction on 8 CCM and 8 control specimens revealed significant downregulation of mRNA expression of occludin, claudin-5, ZO-1, and GLUT-1. The altered expression and localization of the TJPs at interendothelial contact sites accompanied by a reduction of GLUT-1 expression in dilated CCM microvessels likely affect vascular matrix stability and may contribute to hemorrhages of CCMs.

DOI: https://doi.org/10.1097/NEN.0b013e31821bc40e

Editorial Manager(tm) for Journal of Neuropathology and Experimental Neurology
Manuscript Draft

Manuscript Number: JNEN 10-322R1

Title: Impairment of tight junctions and glucose transport in endothelial cells of human cerebral cavernous malformations.

Article Type: Original Study

Keywords: cerebral cavernous malformation, tight junctions, occludin, claudin-5, ZO-1, GLUT-1

Corresponding Author: Hannah Schneider, Ph.D.

Corresponding Author's Institution: University Hospital

First Author: Hannah Schneider, Ph.D.

Order of Authors: Hannah Schneider, Ph.D.;Mariella Errede, Ph.D.;Nils H. Ulrich, M.D.;Daniela Virgintino, M.D., Ph.D.;Karl Frei, Ph.D.;Helmut Bertalanffy, M.D.

Abstract: Cerebral cavernous malformations (CCMs) often cause hemorrhages which can result in severe symptoms like hemiparesis or seizures. The underlying mechanism behind the aggressive behavior of a CCM lesion is undetermined to date, but alterations of vascular matrix components may be responsible. Hence, we investigated the localization of the tight junction proteins (TJPs) occludin, claudin-5 and ZO-1 within endothelial cells. Additionally, we examined the expression of glucose transporter 1 (GLUT-1) which is sensitive to alterations in TJP levels. Seven CCM and five control (normal brain tissue) specimens were examined by fluorescent immunohistochemistry for occludin, claudin-5, ZO-1 and GLUT-1. Our protein expression analysis showed that occludin, claudin-5 and ZO-1 were downregulated at intercellular contact sites and partly redistributed within the surrounding tissue in all patients examined. We also observed a massive reduction of GLUT-1 that was not observed in any of the control specimens. Corresponding analysis using quantitative real-time RT-PCR (qRT-PCR), revealed a significant downregulation in mRNA-expression of occludin, claudin-5, ZO-1 and GLUT-1.

*Cover Letter with Response to Reviewers

Universitätsspital Zürich

Klinik für Neurochirurgie

Raymond A. Sobel, MD
Editor-in-Chief
Journal of Neuropathology& Experimental Neurology
Department of Pathology
Stanford University Medical Center
Pathology and Laboratory Service (113)
Veterans Affairs Health Care System
3801 Miranda Avenue
Palo Alto, CA 94304

Dr. H. Schneider
wissenschaftl. Mitarbeiterin
Universitätsspital Zürich
Klinik für Neurochirurgie
Frauenklinikstr. 10
CH-8091 Zürich

Phone +41-44-2559828
Fax +41-44-2554514
E-mail:
hannah.schneider@usz.ch

Zurich, 3rd March, 2011

RE: JNEN 10-332

Dear Professor Sobel,

Please find attached our revised manuscript entitled:

„ *Impairment of tight junctions and glucose transport in endothelial cells of human cerebral cavernous malformation"*

by H. Schneider, N. H. Ulrich, M. Errede, D. Virgintino, K. Frei and H. Bertalanffy.

Due to the reviewers concerns, you considered a revised manuscript if we satisfactorily address their queries, criticisms and suggestions. This revised manuscript takes into account the reviewers concerns, which we address in a detailed point-by-point reply, which you can find below.

Our data revealed that improper tight junction assembly reflects a hallmark in the pathogenesis of cerebral cavernous malformations (CCM). There is strong evidence that we could identify proteins that are responsible for the resulting vascular matrix instability seen in CCM, which might lead to hemorrhage into the surrounding brain tissue.

As already mentioned, we focused our analysis on cell biological differences regulating the BBB under physiological conditions compared to the situation in CCM pathology. This is in contrast to previous studies in CCM focusing mainly on the genetic mutations of *CCM genes 1, 2* and *3.*

Our findings are of particular importance for the molecular understanding of CCM pathophysiology because obvious alterations in tight junction assembly and metabolic processes in endothelial cells in examined lesions may contribute to a new pathophysiological process and present a possible therapeutic concept in the future.

We would be grateful if you would consider our reviewed manuscript for publication in your journal.
We assure you that neither the submitted material herein nor portions thereof have been published previously or are under consideration for publication elsewhere and hence present no conflicts of interest.

Sincerely yours,

Hannah Schneider

Reply to the Referees' Comments:

Reviewer #1:

In this revised version the problem with Figures 1-3 persists. The authors included immunostaining for CD31 as suggested, however, the high magnification of the images still does not allow the reader to identify endothelia of a cavernoma. Fig. 1 A for example shows a small vessel surrounded by many cells of unknown identity. This feature is not typical for a cavernoma since the vessel is very small, only about four nuclei in diameter. Typical cavernoma vessels are larger and one vessel neighbors the next. The same holds true for Figure 5. The vessels in A, B and C seem to be dilated capillaries and are not typical for cavernoma vessels.

Now, we additionally included comparable figures of paraffin sections stained for occludin and GLUT-1 on one of the studied cases. These two figures are put within the revised manuscript as supplemental figures (Fig. S1 and S2) and are mentioned within the results section. The diameters of the vessels shown in the images are bigger compared to some of the vessels shown in figures 1-6, reflecting more clearly dilated capillaries in CCM tissue. In literature, CCM is defined as a vessel malformation where one vessel neighbors the next. We often observed that dilated capillaries are surrounded by an extracellular matrix-like material (containing collagens). Those ECM-like layers can have a large extend why it is possible to get the impression of "single" vessels although one neighbours the next.

2 - In the discussion the authors provide a hypothesis for the discrepancy between the fluorescence intensitiy (FI) and the microarray data. Since the samples come from different sets of cavernomas, the discrepancy might as well indicate that the results are not representative for cavernomas in general.

We decided to additionally analyze gene expression with quantitative real-time RT-PCR. We suggest that different results of protein and RNA expression might came from the fact, that control tissues used for the two experiments were different: superficial temporal arteries (STAs) for microarrays vesus normal brain tissue (NBT) for immunohistochemistry. mRNA expression was analyzed using eight NBTs and eight CCMs (among them tissue of cases studied in IHC). We could show that mRNA is downregulated for all proteins we analyzed and herewith strengthens our protein data. STA might not be an adequate control tissue, since it doesn't reflect a microvessel phenotype as dilated CCM vessels do. The composition of big arteries is different to the composition of microvessels including gene and protein expression patterns. This could explain different results for gene expression between microarrays and qRT-PCR experiments. We decided to remove the microarray data out of the manuscript and therefore also had to remove the two responsible authors.

Reviewer #2:

It is credible that the TJ proteins occludin, claudin-5 and ZO-1 become redistributed in CCM. Additionally, the expression of adherens junction (AJ) proteins should be shown in particular as CCM1/Krit1 interacts with beta-catenin to assemble the junctional complex. In this respect the available literature (Serebriiskii et al., 1997; Glading et al., 2007; Voss et al., 2007, etc.) should be cited and discussed with regard to the present data.

We discussed this issue but we did not examine our samples for beta-catenin or further adherens junction proteins. This topic is very interesting and since AJ cross-react with TJ, we agree that AJP should be also analyzed in CCM tissue. Then, also studies of mRNA expression and interactions between would be necessary to find out more about how those structures are impaired in the context of CCM pathology. Therefore we decided to put this on the list for future publications.

The authors discuss the distributed staining of TJ protein around CCM blood vessels as "surrounding parenchymal staining". However, these could well be endothelial cells detached from the vessels. PECAM/CD31 might not be the best marker to evaluate co-localization in this case as it is also junctional localized and hence redistributed in CCM. vWF could be an alternative.

We did additional vWF staining as EC-marker together with occludin and GLUT-1, which can be found in the supplemental figures (Fig. S1 and S2).

In general it would be advisable to add an inscription at least to figures 1-4, making it much easier to understand. Furthermore, the order of the figures named in the text should be consecutive. Most prominently, the authors describe the GLUT-1 expression in the second section of the "Results" part, referring to Figure 4 although in the first section they end with Figure 6.

We added inscriptions in Fig. 1-6 to make it easier to understand. And we also changed the order of Fig. 4-6, now being in a consecutive order as named in the text.

As the authors make the point that concomitantly with GLUT-1 misexpression the blood-brain barrier is hampered, it would be informative to stain the CCM samples for human IgG and/or fibronectin to evaluate vessel leakage.

We co-stained CCM and control tissue for fibronectin and EC-marker coll VI (Fig. 7). In contrast to NBT, where fibronectin is located homogenously along vessel walls, the staining pattern is very irregular in CCM tissue reflecting vessel leakage.

With regard to the microarray analysis, it would be important to validate the finding by quantitative RT-PCR analysis.

This we did and results are shown in Fig. 9. Above, we already commented on that issue.

Impairment of tight junctions and glucose transport in endothelial cells of human cerebral cavernous malformations.

Hannah Schneider, Ph.D.[1,+], Mariella Errede, Ph.D.[2], Nils H. Ulrich, M.D.[1], Daniela Virgintino, M.D., Ph.D.[2], Karl Frei, Ph.D.[1], Helmut Bertalanffy, M.D.[1]

(1) Department of Neurosurgery, University Hospital, Zurich, Switzerland

(2) Department of Human Anatomy and Histology, Bari University Medical School, Italy

(+) Hannah Schneider

phone: +41-44-2559828

fax: +41-44-2554505

email: hannah.schneider@usz.ch

Abstract

Cerebral cavernous malformations (CCMs) often cause hemorrhages which can result in severe symptoms like hemiparesis or seizures. The underlying mechanism behind the aggressive behavior of a CCM lesion is undetermined to date, but alterations of vascular matrix components may be responsible. Hence, we investigated the localization of the tight junction proteins (TJPs) occludin, claudin-5 and ZO-1 within endothelial cells. Additionally, we examined the expression of glucose transporter 1 (GLUT-1) which is sensitive to alterations in TJP levels. Seven CCM and five control (normal brain tissue) specimens were examined by fluorescent immunohistochemistry for occludin, claudin-5, ZO-1 and GLUT-1. Our protein expression analysis showed that occludin, claudin-5 and ZO-1 were downregulated at intercellular contact sites and partly redistributed within the surrounding tissue in all patients examined. We also observed a massive reduction of GLUT-1 that was not observed in any of the control specimens. Corresponding analysis using quantitative real-time RT-PCR (qRT-PCR), revealed a significant downregulation in mRNA-expression of occludin, claudin-5, ZO-1 and GLUT-1.

Keywords: cerebral cavernous malformation, tight junctions, occludin, claudin-5, ZO-1, GLUT-1

Introduction

Cerebral cavernous malformations and arteriovenous malformations (AVMs) present the most common lesion subtypes of vascular malformations of the brain (VMBs), affecting more than 0.5% of the population (1-4). CCMs are composed of dilated, blood filled capillary clusters lined by endothelium, lacking intervening brain parenchyma. Due to the expression of angiogenic factors, they reflect more a developing rather than a mature vessel phenotype (1, 3, 5-7). Cavernous malformations occur sporadically, as a single lesion, or as an inherited, autosomal dominant form with multiple lesions (8). To date, mutations in three genes have been identified to cause the familial form of the disease: *CCM1/KRIT1*, *CCM2/MGC4607* and *CCM3/PDCD10* (9). It has been hypothesized that a second hit in the somatic allele is necessary to cause CCM formation. Indeed, in 2005, a biallelic *CCM1* somatic and germ line mutation has been shown in a surgically excised human lesion for the first time (10). In the meantime, biallelic mutations were also reported for *CCM2* and *CCM3* (11). Furthermore, transgenic mice heterozygous for *Ccm1*, only develop CCM lesions when they exhibit an additional homozygous knockout of the tumor suppressor gene *Trp53* ($ccm1^{+/-}$ $Trp53^{-/-}$). Similarly, heterozygous mice with $Ccm2^{\pm}$ only form CCM lesions when sensitized by a second hit (12, 13). This further supports the hypothesis of a second genetic somatic mutation in CCMs.

Recently, it was shown that CCM1 represents an antiangiogenic protein and that gene mutations in *KRIT1* correlate with excessive capillary sprouting, which is characteristic for human CCM pathology (7). PTEN promoter methylation, HEG transmembrane receptor expression, RhoA GTPase and ROCK activation are involved in the pathogenesis (14-17) and therefore have also been suggested to contribute to the mechanism of lesion formation.

Endothelial cells (ECs) are the major component of vessel walls. It is thought that they play a central role in the clinical behavior of a cerebral vascular malformation showing abnormal ultrastructural pathological features (18). The thin walls of CCM vessels possess limited number of intact interendothelial tight junctions, which may contribute to the propensity of recurrent microhemorrhage seen in CCMs (19). There is growing evidence that an impairment of the blood-brain barrier (BBB) correlates with a decrease of tight junctions in the endothelial layer and furthermore that CCM1 as

well as CCM2 could play a junction stabilizing role (15, 17, 20, 21). Recently, it was shown TJP occludin to be involved in intercellular gap formation reflecting BBB breakdown in porcine brain capillary endothelial cells (22).

Tight junctions are located at the lateral apical side of the cell membrane in regions of close cell–cell contacts, e.g. in the cerebral microcapillary endothelium. They turn cell-to-cell contacts into zones of tight adherence thereby inhibiting the paracellular pathway for drugs or solutes from plasma into the central nervous system (CNS) (23). Different integral membrane proteins, associated cytoplasmatic proteins and extracellular matrix components are involved in the proper assembly of tight junction complexes (24). Two junctional core proteins, occludin and claudin-5 play a key role in BBB integrity in the microvascular endothelium. Both consist of four transmembrane domains, intracellular N- and C-termini, and two extracellular domains that might interact with cell membranes of vicinal cells thus sealing the intercellular clefts (22, 25, 26). Different gain-of-function and loss-of-function experiments reveal that claudin-5 is involved in the structure of TJ strands and cell adhesion, whereas occludin probably has some accessory functions (27). Furthermore, adaptor/scaffold proteins such as zonula occludens (ZO-1, ZO-2 and ZO-3) connect TJ-associated integral membrane proteins to the actin cytoskeleton and other structural proteins. The first reported linker protein, ZO-1 directly interacts with occludin and claudins and is essential for TJ formation (27, 28). It was hypothesized that the interaction of occludin with ZO-1 modulates its function in sealing the junction, since paracellular permeability increases when an imbalance occurs between occludin and ZO-1 molecules (29, 30).

The localization of glucose transporter 1 (GLUT-l) in ECs of microvessels is considered as an indicator of a functioning BBB (31-33). The protein is widely expressed in adult tissues, but it is most abundant in fibroblasts, erythrocytes and endothelial cells with low levels of expression in muscle, liver and adipose tissue (34-36). In healthy brain endothelium, TJ sealing of the interendothelial clefts is linked to the expression of GLUT-1. Alterations in transporter protein expression are directly related to an increased permeability of endothelial layers in the brain and also linked to alterations in TJ properties (31-33).

To date, the role of TJs and their core proteins occludin and claudin-5 are not fully understood in the context of CCM lesions. But there is growing evidence that vascular development and endothelial

permeability are dysregulated (37). In brain tumor pathology it was shown, that decreased expression of GLUT-1 is coupled to alterations in TJP expression levels and consequently BBB opening (38). Therefore, we analyzed the expression of TJPs (occludin, claudin-5 and ZO-1) and the transporter protein GLUT-1 by classic immunohistochemistry and confocal fluorescent microscopy on cryo- and paraffin-sections of seven CCM specimens and five control samples (normal brain tissue; NBT). NBT specimens were received from temporal lobe biopsy during selective amygdalohippocampectomy from patients with temporal lobe epilepsy (TLE). Mean fluorescence intensity was further quantified. Furthermore, qRT-PCR was also performed to compare mRNA expression levels of TJPs and GLUT-1 in eight CCM versus eight control samples.

Materials and Methods

Patients and tissue specimens

Twelve CCM specimens were obtained from patients undergoing neurosurgical resection. Thirteen human control tissue specimens (NBT) were received from temporal lobe biopsy during selective amygdalohippocampectomy from patients with TLE. The median age of the seven female and five male patients was 38 (range 23 to 52 years). The clinical data of the twelve CCM patients is summarized in Table 2. List of patients included in this study is based on the consensus recommendations for minimal reporting variables in CCM clinical research (39-41). The decision for surgical resection was made based on computed tomography scan and magnetic resonance imaging. Tissue specimens were immediately transferred to the laboratory on ice and divided for snap-frozen preparation and *in vitro* experiments. Samples were snap-frozen in liquid nitrogen (NO_2) and embedded in TissueTek O.C.T (Satura Finetek Europe, Zoeterwoude, Netherlands) before analysis. Additionally, histological diagnosis was obtained by routine clinical neuropathological examination and classified according to the World Health Organization standards (Institute of Neuropathology, University Hospital Zurich, Switzerland).

Immunofluorescence, laser scanning confocal microscopy and fluorescence microscopy analysis

Immunofluorescence analysis was done by three different protocols. First, 6 µm cryosections were cut with a Leica cryostat, mounted on Superfrost®Plus slides (Menzel-Glaser, Braunschweig, Germany), fixed with acetone p.a. for 10 min at room temperature (RT) and stored at -80°C till further use. For analysis, slides were acetone-fixed for 5 min at RT and air-dried. Sections were incubated with 3% peroxide to quench endogenous peroxidase activity and washed with PBS (pH 7.4). Unspecific binding sites were blocked with blocking solution (Candor, Weißensberg, Germany) for 25 min at RT. For indirect immunofluorescence, polyclonal rabbit anti-human claudin-5-antibody (5 µg/ml; Abcam, Cambridge, UK), monoclonal mouse anti-human occludin-antibody (4 µg/ml; Invitrogen, Carlsbad, CA USA), monoclonal mouse anti-human GLUT-1-antibody (1 µg/ml; Abcam, Cambridge, UK), monoclonal mouse anti-human fibronectin (2 µg/ml; Abcam, Cambridge, UK), mouse monoclonal

anti-human CD31 (10µg/ml; DAKO, Glostrup, DK), monoclonal rabbit anti-human CD31 (1:40; epitomics, Burlingame, CA, USA), monoclonal mouse anti-human collagen-IV-antibody (2 µg/ml; DAKO, Glostrup, DK) and polyclonal rabbit anti-human collagen-VI-antibody (2 µg/ml; Abcam, Cambridge, UK) were incubated at 37°C for 1h. Appropriate secondary antibodies, ALEXA 488-conjugated (goat anti-rabbit and goat anti-mouse 1:100, Invitrogen, Carlsbad, CA, USA) or ALEXA 594-conjugated secondary antibody antibody (goat anti-rabbit and goat anti-mouse, 1:100, Invitrogen Carlsbad, CA, USA) were incubated for 25 min at RT. All antibodies were diluted in "Antibody Dilution Buffer" (DCS, Hamburg, Germany). Between each step, the sections were washed in PBS three times 5 min each. Control stainings included the isotype matched primary monoclonal antibodies. In all cases, the result of each negative control confirmed the specificity of the corresponding antibody staining. Specimens were mounted in fluorescent mounting medium (DAKO, Glostrup, DK) and sections were viewed on a Leica TCS SP5 (Leica, Wetzlar, Germany) confocal laser scanning microscope (CLSM) using 63x and 100x objectives. Confocal images were taken at 1-2 µm intervals through the z-axis of the section. Projection images formed by serial optical planes were analyzed, digitally recorded, and stored as tagged image file format files using Adobe Photoshop CS3 software (Adobe Systems, San Jose, CA, USA). Second, tissue samples were placed into 4% neutral buffered formalin for twelve hours, and then were processed routinely for paraffin inclusion. Sections were obtained at 4 µm intervals using a Microm rotary microtome (Leica, Wetzlar, Germany), put in water and mounted to Superfrost®Plus slides (Menzel-Glaser, Braunschweig, Germany). After rehydration, for antigen retrieval, sections were boiled in a microwave oven in 0.01M citrate buffer solution (pH 6) for 20 minutes. Endogenous peroxidase was inactivated with 3% hydrogen peroxide and nonspecific antigenic sites were blocked with blocking solution (Candor, Weißensberg, Germany) for 25 minutes at RT. As already described above, sections were incubated with primary occludin- (4 µg/ml, Invitrogen, Carlsbad, CA, USA), GLUT-1- (1 µg/ml; Abcam, Cambridge, UK) and polyclonal rabbit anti-human vWF-antibodies (28.5 µg/ml; DAKO, Glostrup, DK) followed by incubation with appropriate secondary antibodies, ALEXA 488-conjugated (goat anti-mouse 1:100, Invitrogen, Carlsbad, CA, USA) or ALEXA 594-conjugated secondary antibody antibody (goat anti-rabbit, 1:100, Invitrogen, Carlsbad, CA, USA). Third, tissue specimens were fixed for 3 h at 4°C by immersion in

2% paraformaldehyde plus 0.2% glutaraldehyde solution and washed in PBS (pH 7.6). The blocks of tissue were sectioned at 20 μm thickness using a vibrating microtome (Leica, Wetzlar, Germany) and sections were collected on polylysine slides (Menzel-Glaser, Braunschweig, Germnay). Heat-mediated antigen retrieval was achieved by microwave pre-treatment in 0.01 M citrate buffer (pH 6.0) for 15 min at 750W. Sections were incubated with PBS/0.5% Triton X-100 for 30 min, blocked with protein block serum free (DAKO, Glostrup, DK) for 15 min at RT and incubated overnight at 4 °C with primary antibodies at various dilutions: mouse monoclonal anti-human claudin-5 (1:20; Zymed Laboratories, Invitrogen, Carlsbad, CA, USA), rabbit polyclonal anti-human occludin (1:50; Zymed Laboratories, Invitrogen, Carlsbad, CA, USA), rabbit polyclonal anti-human collagen IV (1:200; Acris Antibodies GmbH, Hiddenhausen, Germany), mouse monoclonal anti-human collagen IV (1:50; DAKO, Glostrup, DK) and mouse monoclonal anti-human CD31 (1:50; DAKO, Glostrup, DK). A mixture of biotinylated horse anti-mouse (1:400; Vector, Vector Laboratories, Inc.; Burlingame, CA, USA) or biotinylated goat anti-rabbit IgG (1:400; Vector, Vector Laboratories, Inc.; Burlingame, CA, USA) and Alexa568-conjugated goat anti-rabbit (1:400, Invitrogen, Carlsbad, CA, USA) or Alexa555-conjugated goat anti-mouse IgG (1:400, Invitrogen, Carlsbad, CA, USA) were incubated as secondary antibodies for 40 min at RT. Streptavidin Alexa Fuor 488-conjugated (1:400; Invitrogen, Carlsbad, CA, USA) was used for staining of claudin-5 and occludin. The slices were counterstained with TO-PRO-3 (1:10.000 in PBS; Invitrogen, Carlsbad, CA, USA) and finally mounted with Vectashield (Vector Vector Laboratories, Inc.; Burlingame, CA, USA) and sealed with nail varnish. The stainings were examined under the Leica TCS SP5 confocal laser scanning microscope (Leica, Wetzlar, Germany) using a sequential scan procedure during image acquisition of double-labeled sections. Confocal images were taken at 250-500 nm intervals through the z-axis of the sections. Images from individual optical planes and image projections of stacks of serial optical planes were analyzed by Leica confocal software (Multicolor Package; Leica, Wetzlar, Germany).

Image Acquisition, image processing and data analysis

Digital image processing for the detection and quantification of fluorescent intensitiy (QFI) in human CCM and control samples was performed with a conventional light microscope (Axiovert 100, Zeiss,

Jena, Germany), a digital microscope camera (AxioCam ICm, Zeiss, Jena, Germany) and the AxioVision 4.8 software (Zeiss, Jena, Germany). Fluorescence quantification was sub-divided into image acquisition, image preprocessing, and data processing steps (42). All parameters used in the acquisition were standardized (detector gain, exposure time) to maintain high reproducibility. Image processing of each specimen was provided through region of interest (ROI) analysis. The software allows the interactive definition of areas for size and intensity measurements. For data analysis, fluorescence intensity/ROI values were obtained for five ROIs/specimen (10 μm^2 each). Statistical analysis describing the distribution of the intensity of the fluorescence signals was performed to obtain graphical representations.

Quantitative RT-PCR analysis

Differential gene expression levels of claudin-5, occludin, ZO-1 and GLUT-1 were determined by q RT-PCR. Therefore, total RNA was isolated from each cavernoma and control tissue sample using the RNeasy Mini Kit Isolation System according to the manufactor's protocol for RNA extraction (Qiagen Ltd., Hombrechtikon, Schweiz). 0.5 µg total mRNA of each sample was reverse transcribed to cDNA using the High Capacity cDNA Reverse Transcription Kit (ABI, Carlsbad, CA, USA). cDNA was used for qRT-PCR with SYBR® Green PCR Master Mix (ABI, Carlsbad, CA, USA) and specific primer pairs on a 7900HT Fast Real-Time PCR System with SDS Software v2.4 (ABI, Carlsbad, CA, USA). Expression was normalized against the endothelial marker CD31 or vWF. Specific primers were designed with the Primer Express 3.0 software (ABI, Carlsbad, CA, USA) and are listed in Table 1.

Statistical analysis

For quantification and statistical analysis of protein expression levels, experiments were done in triplicates analyzing five ROIs/specimen ($10\mu m^2$) for each patient. Mean fluorescence intensity (MFI) values were calculated and averaged. ROIs were selected randomly by criteria that only fluorescent signals of vessel wall structures were measured for their intensity. The statistical analysis, using the mean fluorescence intensity values of each patient, was performed with Microsoft Excel and GraphPad Prism software (version 5 for Windows). To assess whether two independent samples of observations come from the same distribution, an unpaired students *t*-test was used. P-values < 0.01 were considered as statistically significant.

mRNA expression levels of each gene were obtained via correction for endothelial density. The results are expressed as means ± standard error (SEM). Statistical evaluation was performed with GraphPad Prism software (version 5 for Windows). Statistical significance was determined by Mann-Whitney-Wilcoxon Test . P-values < 0.05 were considered as statistically significant.

Results

Comparison of TJPs between CCM and NBT microvessels

Initially, protein expression patterns of TJPs occludin, claudin-5 and ZO-1 from seven CCM and five control specimens were examined on intact vascular structures by fluorescent immunohistochemistry and analyzed via laser scanning confocal microscopy (representative images of following samples are shown: Fig. 1: CCM#1, CCM#2, c#2 and c#4; Fig. 2: CCM#2,CCM#3, c#2 and c#4; Fig. 3: CCM#2, CCM#3, c#1 and c#4 and Fig. S1: CCM#1, c#1). The levels of TJP expression were compared to control tissues obtained from patients with temporal lobe epilepsy who had undergone surgery. Representative results for two CCM and control specimens, respectively, are shown in Figs. 1-3 and S1. To identify endothelial cells (ECs), sections were co-stained for the EC marker protein PECAM-1/CD31 on cryosections (Fig.1-3: A''-D'') and von Willebrand factor (vWF) on paraffin sections (Fig. S1: A''-D''). Protein expression of occludin, claudin-5 and ZO-1 was clearly decreased in endothelial layers of CCM tissue compared to control brain microvessels, which showed a typical linear staining pattern at distinct endothelial cell borders. The linear junctional labeling was either discontinuous or amorphous and many vessels even appeared negative for TJPs. In several cases, redistribution of proteins was observed in the endothelial layer as well as the surrounding tissue (Fig. 1-3: A'-C'). Co-staining for CD31 and vWF additionally revealed that only microvessels were analyzed for impairment in TJP localization.

We then proceeded to build three dimensional reconstructions of vascular structures to validate the immunofluorescence experiments which showed different localization patterns for TJPs along the margin of cell–cell contacts and in the surrounding tissue of CCMs when compared to controls (Fig. 4 and 5). In CCM tissue, in regions where a protein signal could be determined, few vessels showed a punctuate labelling for claudin-5 (Fig. 4B/C and 5A/B), in others occludin and claudin-5 were linearly arranged along the endothelial cell-cell contacts as it was observed in the vessels of control tissues (Fig. 4A; Fig. 5C). In those cases, the fluorescence signal of both proteins was clearly weakened compared to the signal intensity in healthy tissue. Furthermore, in vessels of control tissues, occludin

and claudin-5 staining was limited to the vascular intima (Fig. 4D/E and 5D), whereas it could also be detected in the surrounding tissue in some regions of the CCM sections (Fig. 5A).

GLUT-1 expression in CCM vessels

Alterations in transporter protein expression are directly related to an increased permeability of endothelial layers in the brain and also linked to alterations in TJ properties (31-33).

To investigate BBB permeability, which not only corresponds to alterations in TJPs but to an impairment of GLUT-1 expression, we also stained CCM and control tissue cryosections for this transmembrane transporter protein (shown in Fig. 6 for samples: CCM#1, CCM#6, c#1 and c#5 on cryosections and Fig. S2: CCM#3, c#1 on paraffin embedded sections). We could observe that microvessels of control brain tissues were stained uniformly and showed a high level of GLUT-1 expression (Fig. 6 and S2: C'-D'). Unlike in controls, GLUT-1 expression was reduced or absent in CCM specimens (Fig. 6 and S2: A'-B'). As an internal positive control, erythrocytes were stained in every sample, to reflect membranous GLUT-1 activity (Fig. 6 and S2: B'). To conclude, linear TJP localization at EC boarders was clearly disrupted and accompanied by a massive reduction of GLUT-1 staining. This reflects an impairment of the BBB, which is supported by vessel leakage illustrated in Fig. 7 by an irregular fibronectin staining around CCM microvessels.

Alterations in TJP and GLUT-1 expression in CCMs

For further analysis, alterations in protein expression levels were quantified by determining signal intensities of immunofluorescent labeled cryosections of CCM against the intensities in control specimens. As described above, a strong reduction of TJP and GLUT-1 levels were observed along EC cell borders, corresponding to decreased FI per ROI (Fig. 8). A drop of occludin-, claudin-5-, ZO-1- and GLUT-1-fluorescence signal was determined in each CCM specimen (Fig. 8A). Slight differences in the extent of protein reduction are due to unique tissue composition of each CCM sample. Mean values, calculated for CCMs and controls, revealed a FI signal reduction of 62% for occludin, 71% for claudin-5 and 74% for ZO-1 in CCM tissue compared to those in control tissue (Fig. 8B). The

decrease of fluorescence intensity/protein expression in CCM vessels was found to be highly significant in all cases ($p < 0.0001$, ****).

Hence, the most striking decrease of protein expression in pathologic vessels was found for GLUT-1 (78%). Again, reduction was determined as highly significant by an unpaired students *t*-test ($p < 0.0001$, ****).

mRNA expression analysis of occludin, claudin-5, ZO-1 and GLUT-1 in CCMs

As shown above, protein levels of TJPs occludin, claudin-5, ZO-1 and glucose transporter GLUT-1 are downregulated at intercellular contact sites and in microvessels of CCMs, respectively. In order to validate those findings, we performed real-time RT-PCR and normalized against either endothelial marker CD31 (Fig. 9) or vWF (not shown), showing similar results. Total RNAs from eight samples were analyzed for each group (CCM and NBT). RNA expression of occludin (13±3.6%), claudin-5 (25.8±8.3%) and ZO-1 (8.2±3.6%) was significantly decreased in CCM versus to NBT samples (Mann-Whitney-Wilcoxon-Test, $p < 0.05$). Similarly, GLUT-1 was also significantly reduced (15.8±4.3) when compared with RNA expression in NBT.

Discussion

In this study, we discovered that tight junction proteins occludin, claudin-5, ZO-1, and glucose transporter protein GLUT-1 compositions are impaired in CCM tissue. Expression of these proteins was strongly reduced at interendothelial contact sites, and appeared negative in most of the vessels.

In healthy endothelial layers, correct assembly of TJs is essential for the maintenance of a functional permeability barrier. It is known, that the structural composition of TJs in ECs of brain capillaries is the most complex among any other physiological systems (43). Therefore, it is suggested that an impairment of TJ assembly can lead to a loss of BBB integrity (44-46). Furthermore, localization of GLUT-1 is considered to be an excellent indicator of a normally functioning BBB (31-33). We therefore investigated the expression of TJPs and GLUT-1 to get more information about subcellular events leading to an aggressive behavior of a CCM lesion. In fact, occludin and claudin-5, which are critical for proper BBB function and permeability (45, 47, 48), are downregulated at interendothelial contact sites in CCM tissue. Furthermore, we observed that TJ-associated protein ZO-1 expression was also altered. ZO-1 and occludin are considered to be the most important protein components for the maintenance of the barrier function of brain microvessels (49-51). Additionally, previous studies have found occludin to play an important role in the regulation of brain capillary permeability (52). Other studies show that claudin-5 plays an essential role in TJ formation generating the structural and functional core of the multiprotein complex (27). Our findings, of deviations in TJP localization, are accompanied by clear protein redistribution within the surrounding brain parenchyma of CCM vessels. The resulting incorrect assembly of TJs may lead to a malfunction of proper BBB. Moreover, downregulation of ZO-1 suggests a disturbance in interaction of TJs with the actin cytoskeleton, strongly assuming a direct influence in the pathology of CCMs. This may lead to the possibility of a disruption in the cellular architecture, which may consequently lead to decreasing cellular stability. It is known, that downregulation of ZO-1 in CCMs results in a mismatch between interacting TJPs. Furthermore, overexpression of occludin and inadequate levels of ZO-1 enhance the impairment of the BBB (29). Additionally, occludin phosphorylation correlates with TJ formation and regulation of junction permeability and interaction with ZO-1 (53-55). As claudin-5 is a key determinant of trans-

endothelial resistance at the BBB, alterations in its interacting proteins can also lead to a disruption of the barrier function (53).

Taken together, our observations give strong evidence that cell-cell contacts of CCM vessels are disorganized to some extent and that TJ proteins are redistributed in parts of the EC surrounding tissue. These observations suggest an alteration of tight junction assembly in CCMs leading to a malfunctioning permeability barrier, like it is reported in brain tumor vessels or in brain microcapillaries after ischemic events (22, 38, 56). And indeed, in many patients, CCM pathology comprises repeated microhemorrhages into the surrounding brain parenchyma corresponding to an impaired permeability of brain capillaries. Recently, it was shown in a CCM mouse model, that heterozygosity at *Ccm2* locus impaired endothelial barrier function via alterations in cell-to-cell interactions, cytoskeletal architecture and lumen formation (15). In addition, loss of CCM1 results in disruption of junctional stability that leads to increased permeability *in vitro* and *in vivo*. It also has been shown that the activation of the Rho GTPase RhoA and its downstream effector ROCK, in turn, caused by a loss of CCM1 and CCM2, influences vascular leakage (15, 17). Therefore, most likely either direct and linker protein mediated interactions between CCM1/CCM2 and TJPs probably exist.

However, it has to be mentioned, that CCM vessels are not devoid of correctly assembled TJ complexes, even though expression was weakened, linear staining patterns of occludin, claudin-5 and ZO-1 could still be observed along the endothelial cell-cell contacts in very few CCM foci. Therefore, further examinations must be carried out to investigate whether higher percentage of linear TJP arrangement at cell-cell-boarders correlates with the aggressive clinical behavior of a lesion, as already suggested by other groups (20, 57).

Quantification of signal intensities of TJP expression confirmed our initial immunohistochemical observation. Downregulation of occludin, claudin-5 and ZO-1 in regions of interendothelial contact sites has been shown to be highly significant and strongly validates the assumption that TJP are critical for the barrier function of brain vasculature and thus disruption of their expression leads to an impairment of BBB function.

We also investigated the expression pattern of GLUT-1 within CCMs, since it was shown that alterations of TJP was paralleled by a reduction of GLUT-1 in cerebral endothelial cells and is

consistent with BBB opening in tumor tissues (31-33, 38). Furthermore, it is known, that BBB breakdown occurs in human CCMs and is, amongst others, thought to be responsible for aggressive behavior of a lesion (20, 57). However, an underlying mechanism leading to an expansion and rupture of a CCM lesion, remains a mystery (58). As already expected, alterations in TJP distribution was accompanied by a massive downregulation of GLUT-1, which is found to be highly significant. This effect was accompanied by an irregular fibronectin staining which reflects vessel leakage. In most CCM vessels, GLUT-1 is completely absent and with positive signal being detectable in erythrocytes only. Staining of red blood cells in extravascular CCM tissue either indicates recent hemorrhage and serves as an internal positive control. GLUT-1 is the only known endothelial BBB glucose transporter protein, therefore its downregulation is probably correlated to impaired glucose uptake into the brain and metabolic rate of cells (59).

Our analysis revealed that the scarcity of in TJP and GLUT-1 protein levels did correspond to modifications in gene expression. Changes in relative amounts of TJP- and GLUT-1-mRNA were evaluated as highly significant. Therefore it appears to be obvious that differences in protein concentrations at TJs and EC plasma membranes are caused by downregulation of mRNA expression. Additionally, to some extent, impaired TJP and GLUT-1 levels in CCM vessels may also correspond to protein redistribution within the tissue which could be influenced by alterations with further binding partners. In this context, impaired interactions with adherens junction components (AJs) could also play a role. The most important element of AJs consists of the VE-Cadherin/β-catenin complex (60). It is known, that CCM1/Krit1 interacts with β-catenin, which in turn shows cross-reaction with TJs, probably in a Rap-1 GTPase-dependent manner (21, 61). Therefore it should be taken into account that alterations in TJPs and GLUT-1 levels could in turn influence or be caused by impairments in AJ protein components.

In conclusion, our data strongly supports the fundamental role of TJ complexes and TJP in the pathogenesis of CCMs. We were able to show that CCM pathology corresponds to an impaired localization of occludin, claudin-5 and ZO-1 at interendothelial contact sites, which is accompanied by a massive reduction of GLUT-1 in dilated CCM microvessels. These findings may affect vascular matrix stability, and thus can contribute to an aggressive clinical behavior seen in CCMs. Future

attempts will need to study the interactions of TJPs with *CCM1, 2* and *3* gene products and other binding partners, for example AJ proteins. Furthermore, more information about the role of TJPs in the formation of a tight BBB in CCM will greatly facilitate a better understanding of lesional behavior and could be beneficial in the development of an appropriate treatment.

Acknowledgments

This research was supported by the Center for Clinical Research at the University of Zurich. The authors thank the Center for Microscopy and Image Analysis, University of Zurich, for the use of the CLSM and technical assistance. The authors thank Mushfika Ahmad (Departments of Neurosurgery and Neurology, University Hospital, Zurich) for meticulous editorial revision and Dr. Johannes Schmitt and Claudia Gottier (Division of Gastroenterology and Hepatology, University Hospital Zurich) for their assistance in RT-PCR performance.

Conflict of interest

The authors declare that they have no conflict of interest.

References

1. Al-Shahi R, Bhattacharya JJ, Currie DG, Papanastassiou V, Ritchie V, Roberts RC, Sellar RJ, Warlow CP. Prospective, population-based detection of intracranial vascular malformations in adults: the Scottish Intracranial Vascular Malformation Study (SIVMS). Stroke 2003e:34;1163-9.

2. Del Curling O, Jr., Kelly DL, Jr., Elster AD, Craven TE. An analysis of the natural history of cavernous angiomas. J Neurosurg 1991e:75;702-8.

3. Rigamonti D, Hadley MN, Drayer BP, Johnson PC, Hoenig-Rigamonti K, Knight JT, Spetzler RF. Cerebral cavernous malformations. Incidence and familial occurrence. N Engl J Med 1988e:319;343-7.

4. Leblanc GG, Golanov E, Awad IA, Young WL. Biology of vascular malformations of the brain. Stroke 2009e:40;e694-702.

5. Rothbart D, Awad IA, Lee J, Kim J, Harbaugh R, Criscuolo GR. Expression of angiogenic factors and structural proteins in central nervous system vascular malformations. Neurosurgery 1996e:38;915-24; discussion 24-5.

6. Kilic T, Pamir MN, Kullu S, Eren F, Ozek MM, Black PM. Expression of structural proteins and angiogenic factors in cerebrovascular anomalies. Neurosurgery 2000e:46;1179-91; discussion 91-2.

7. Wustehube J, Bartol A, Liebler SS, Brutsch R, Zhu Y, Felbor U, Sure U, Augustin HG, Fischer A. From the Cover: Cerebral cavernous malformation protein CCM1 inhibits sprouting angiogenesis by activating DELTA-NOTCH signaling. Proc Natl Acad Sci U S A 2010e:107;12640-5.

8. Mindea SA, Yang BP, Shenkar R, Bendok B, Batjer HH, Awad IA. Cerebral cavernous malformations: clinical insights from genetic studies. Neurosurg Focus 2006e:21;e1.

9. Labauge P, Denier C, Bergametti F, Tournier-Lasserve E. Genetics of cavernous angiomas. Lancet Neurol 2007e:6;237-44.

10. Gault J, Shenkar R, Recksiek P, Awad IA. Biallelic somatic and germ line CCM1 truncating mutations in a cerebral cavernous malformation lesion. Stroke 2005e:36;872-4.

11. Akers AL, Johnson E, Steinberg GK, Zabramski JM, Marchuk DA. Biallelic somatic and germline mutations in cerebral cavernous malformations (CCMs): evidence for a two-hit mechanism of CCM pathogenesis. Hum Mol Genet 2009e:18;919-30.

12. Shenkar R, Venkatasubramanian PN, Wyrwicz AM, Zhao JC, Shi C, Akers A, Marchuk DA, Awad IA. Advanced magnetic resonance imaging of cerebral cavernous malformations: part II. Imaging of lesions in murine models. Neurosurgery 2008e:63;790-7; discussion 7-8.

13. Plummer NW, Gallione CJ, Srinivasan S, Zawistowski JS, Louis DN, Marchuk DA. Loss of p53 sensitizes mice with a mutation in Ccm1 (KRIT1) to development of cerebral vascular malformations. Am J Pathol 2004e:165;1509-18.

14. Kleaveland B, Zheng X, Liu JJ, Blum Y, Tung JJ, Zou Z, Sweeney SM, Chen M, Guo L, Lu MM, Zhou D, Kitajewski J, Affolter M, Ginsberg MH, Kahn ML. Regulation of cardiovascular development and integrity by the heart of glass-cerebral cavernous malformation protein pathway. Nat Med 2009e:15;169-76.

15. Whitehead KJ, Chan AC, Navankasattusas S, Koh W, London NR, Ling J, Mayo AH, Drakos SG, Jones CA, Zhu W, Marchuk DA, Davis GE, Li DY. The cerebral cavernous malformation signaling pathway promotes vascular integrity via Rho GTPases. Nat Med 2009e:15;177-84.

16. Zhu Y, Wloch A, Wu Q, Peters C, Pagenstecher A, Bertalanffy H, Sure U. Involvement of PTEN promoter methylation in cerebral cavernous malformations. Stroke 2009e:40;820-6.

17. Stockton RA, Shenkar R, Awad IA, Ginsberg MH. Cerebral cavernous malformations proteins inhibit Rho kinase to stabilize vascular integrity. J Exp Med 2010e:207;881-96.

18. Zhao Y, Tan YZ, Zhou LF, Wang HJ, Mao Y. Morphological observation and in vitro angiogenesis assay of endothelial cells isolated from human cerebral cavernous malformations. Stroke 2007e:38;1313-9.

19. Wong JH, Awad IA, Kim JH. Ultrastructural pathological features of cerebrovascular malformations: a preliminary report. Neurosurgery 2000e:46;1454-9.

20. Clatterbuck RE, Eberhart CG, Crain BJ, Rigamonti D. Ultrastructural and immunocytochemical evidence that an incompetent blood-brain barrier is related to the pathophysiology of cavernous malformations. J Neurol Neurosurg Psychiatry 2001e:71;188-92.

21. Glading A, Han J, Stockton RA, Ginsberg MH. KRIT-1/CCM1 is a Rap1 effector that regulates endothelial cell cell junctions. J Cell Biol 2007e:179;247-54.

22. Lischper M, Beuck S, Thanabalasundaram G, Pieper C, Galla HJ. Metalloproteinase mediated occludin cleavage in the cerebral microcapillary endothelium under pathological conditions. Brain Res 2010e:1326;114-27.

23. Cornford EM, Hyman S. Localization of brain endothelial luminal and abluminal transporters with immunogold electron microscopy. NeuroRx 2005e:2;27-43.

24. Rosenberg GA, Yang Y. Vasogenic edema due to tight junction disruption by matrix metalloproteinases in cerebral ischemia. Neurosurg Focus 2007e:22;E4.

25. Anderson JM, Van Itallie CM. Tight junctions and the molecular basis for regulation of paracellular permeability. Am J Physiol 1995e:269;G467-75.

26. Tsukita S, Furuse M. Occludin and claudins in tight-junction strands: leading or supporting players? Trends Cell Biol 1999e:9;268-73.

27. Furuse M. Molecular basis of the core structure of tight junctions. Cold Spring Harb Perspect Biol 2010e:2;a002907.

28. Fanning AS, Jameson BJ, Jesaitis LA, Anderson JM. The tight junction protein ZO-1 establishes a link between the transmembrane protein occludin and the actin cytoskeleton. J Biol Chem 1998e:273;29745-53.

29. Feldman GJ, Mullin JM, Ryan MP. Occludin: structure, function and regulation. Adv Drug Deliv Rev 2005e:57;883-917.

30. McCarthy KM, Skare IB, Stankewich MC, Furuse M, Tsukita S, Rogers RA, Lynch RD, Schneeberger EE. Occludin is a functional component of the tight junction. J Cell Sci 1996e:109 (Pt 9);2287-98.

31. Dobrogowska DH, Vorbrodt AW. Quantitative immunocytochemical study of blood-brain barrier glucose transporter (GLUT-1) in four regions of mouse brain. J Histochem Cytochem 1999e:47;1021-30.

32. Gerhart DZ, LeVasseur RJ, Broderius MA, Drewes LR. Glucose transporter localization in brain using light and electron immunocytochemistry. J Neurosci Res 1989e:22;464-72.

33. Lippoldt A, Kniesel U, Liebner S, Kalbacher H, Kirsch T, Wolburg H, Haller H. Structural alterations of tight junctions are associated with loss of polarity in stroke-prone spontaneously hypertensive rat blood-brain barrier endothelial cells. Brain Res 2000e:885;251-61.

34. Birnbaum MJ, Haspel HC, Rosen OM. Cloning and characterization of a cDNA encoding the rat brain glucose-transporter protein. Proc Natl Acad Sci U S A 1986e:83;5784-8.

35. Fukumoto H, Seino S, Imura H, Seino Y, Eddy RL, Fukushima Y, Byers MG, Shows TB, Bell GI. Sequence, tissue distribution, and chromosomal localization of mRNA encoding a human glucose transporter-like protein. Proc Natl Acad Sci U S A 1988e:85;5434-8.

36. Pardridge WM, Boado RJ, Farrell CR. Brain-type glucose transporter (GLUT-1) is selectively localized to the blood-brain barrier. Studies with quantitative western blotting and in situ hybridization. J Biol Chem 1990e:265;18035-40.

37. Yadla S, Jabbour PM, Shenkar R, Shi C, Campbell PG, Awad IA. Cerebral cavernous malformations as a disease of vascular permeability: from bench to bedside with caution. Neurosurg Focus 2010e:29;E4.

38. Ishihara H, Kubota H, Lindberg RL, Leppert D, Gloor SM, Errede M, Virgintino D, Fontana A, Yonekawa Y, Frei K. Endothelial cell barrier impairment induced by glioblastomas and transforming growth factor beta2 involves matrix metalloproteinases and tight junction proteins. J Neuropathol Exp Neurol 2008e:67;435-48.

39. Al-Shahi Salman R, Berg MJ, Morrison L, Awad IA. Hemorrhage from cavernous malformations of the brain: definition and reporting standards. Angioma Alliance Scientific Advisory Board. Stroke 2008e:39;3222-30.

40. Kivelev J, Niemela M, Kivisaari R, Dashti R, Laakso A, Hernesniemi J. Long-term outcome of patients with multiple cerebral cavernous malformations. Neurosurgery 2009e:65;450-5; discussion 5.

41. van Swieten JC, Koudstaal PJ, Visser MC, Schouten HJ, van Gijn J. Interobserver agreement for the assessment of handicap in stroke patients. Stroke 1988e:19;604-7.

42. Di Iorio E, Barbaro V, Ferrari S, Ortolani C, De Luca M, Pellegrini G. Q-FIHC: quantification of fluorescence immunohistochemistry to analyse p63 isoforms and cell cycle phases in human limbal stem cells. Microsc Res Tech 2006e:69;983-91.

43. Nagy Z, Peters H, Huttner I. Fracture faces of cell junctions in cerebral endothelium during normal and hyperosmotic conditions. Lab Invest 1984e:50;313-22.

44. Furuse M, Hirase T, Itoh M, Nagafuchi A, Yonemura S, Tsukita S. Occludin: a novel integral membrane protein localizing at tight junctions. J Cell Biol 1993e:123;1777-88.

45. Nitta T, Hata M, Gotoh S, Seo Y, Sasaki H, Hashimoto N, Furuse M, Tsukita S. Size-selective loosening of the blood-brain barrier in claudin-5-deficient mice. J Cell Biol 2003e:161;653-60.

46. Ohtsuki S, Sato S, Yamaguchi H, Kamoi M, Asashima T, Terasaki T. Exogenous expression of claudin-5 induces barrier properties in cultured rat brain capillary endothelial cells. J Cell Physiol 2007e:210;81-6.

47. Harhaj NS, Antonetti DA. Regulation of tight junctions and loss of barrier function in pathophysiology. Int J Biochem Cell Biol 2004e:36;1206-37.

48. Hawkins BT, Davis TP. The blood-brain barrier/neurovascular unit in health and disease. Pharmacol Rev 2005e:57;173-85.

49. Bolton SJ, Anthony DC, Perry VH. Loss of the tight junction proteins occludin and zonula occludens-1 from cerebral vascular endothelium during neutrophil-induced blood-brain barrier breakdown in vivo. Neuroscience 1998e:86;1245-57.

50. Citi S. The molecular organization of tight junctions. J Cell Biol 1993e:121;485-9.

51. Vorbrodt AW, Dobrogowska DH, Tarnawski M. Immunogold study of interendothelial junction-associated and glucose transporter proteins during postnatal maturation of the mouse blood-brain barrier. J Neurocytol 2001e:30;705-16.

52. Forster C. Tight junctions and the modulation of barrier function in disease. Histochem Cell Biol 2008e:130;55-70.

53. Argaw AT, Gurfein BT, Zhang Y, Zameer A, John GR. VEGF-mediated disruption of endothelial CLN-5 promotes blood-brain barrier breakdown. Proc Natl Acad Sci U S A 2009e:106;1977-82.

54. Kebir H, Kreymborg K, Ifergan I, Dodelet-Devillers A, Cayrol R, Bernard M, Giuliani F, Arbour N, Becher B, Prat A. Human TH17 lymphocytes promote blood-brain barrier disruption and central nervous system inflammation. Nat Med 2007e:13;1173-5.

55. Sakakibara A, Furuse M, Saitou M, Ando-Akatsuka Y, Tsukita S. Possible involvement of phosphorylation of occludin in tight junction formation. J Cell Biol 1997e:137;1393-401.

56. Wachtel M, Bolliger MF, Ishihara H, Frei K, Bluethmann H, Gloor SM. Down-regulation of occludin expression in astrocytes by tumour necrosis factor (TNF) is mediated via TNF type-1 receptor and nuclear factor-kappaB activation. J Neurochem 2001e:78;155-62.

57. Tu J, Stoodley MA, Morgan MK, Storer KP. Ultrastructural characteristics of hemorrhagic, nonhemorrhagic, and recurrent cavernous malformations. J Neurosurg 2005e:103;903-9.

58. Fujimura M, Watanabe M, Shimizu H, Tominaga T. Expression of matrix metalloproteinases (MMPs) and tissue inhibitor of metalloproteinase (TIMP) in cerebral cavernous malformations: immunohistochemical analysis of MMP-2, -9 and TIMP-2. Acta Neurochir (Wien) 2007e:149;179-83; discussion 83.

59. Hou WK, Xian YX, Zhang L, Lai H, Hou XG, Xu YX, Yu T, Xu FY, Song J, Fu CL, Zhang WW, Chen L. Influence of blood glucose on the expression of glucose trans-porter proteins 1 and 3 in the brain of diabetic rats. Chin Med J (Engl) 2007e:120;1704-9.

60. Dejana E, Corada M, Lampugnani MG. Endothelial cell-to-cell junctions. FASEB J 1995e:9;910-8.

61. Birukova AA, Zebda N, Fu P, Poroyko V, Cokic I, Birukov KG. Association between adherens junctions and tight junctions via Rap1 promotes barrier protective effects of oxidized phospholipids. J Cell Physiol 2010e.

Figure Legends

FIGURE 1. Localization of the tight junction protein occludin (green) in CCM specimens: Confocal z-series projections of CCM#1, CCM#2 (A-B) and control samples c#2, c#4 (C-D). Occludin is distributed in a linear pattern along vessels of control tissues (C': cross sectional; D': longitudinal). Occludin is redistributed and shows decreased expression in ECs of CCMs (A': cross sectional; B': longitudinal). The endothelial cell marker protein PECAM-1 (CD31) is stained in red (A''-D''). DAPI (blue) is shown in A-D and merged images in A'''-D'''. Bars: 20 µm.

FIGURE 2. Distribution of TJP claudin-5 (green) and localization of EC-marker CD31 (red: A''-D'') in CCM specimens: CCM#2, CCM#3 (A-B) and controls: c#2, c#4 (C-D) by confocal microscopy. Claudin-5, same as occludin, is distributed linearly in vessels of control tissues (C': cross sectional; D': longitudinal). In CCM endothelial cells, claudin-5 expression is decreased (A' and B': cross sectional). DAPI (blue) is shown in A-D and merged images in A'''-D'''. Bars: 20 µm.

FIGURE 3. Confocal microscopy images of TJP ZO-1 (green) and CD31 (red) of CCMs (CCM#2, CCM#3) and control specimens (c#1, c#4). As in control tissue section stainings for occludin and claudin-5, ZO-1 is distributed in a typical linear vessel pattern (C': cross sectional; D': longitudinal). In contrast, ZO-1 is significantly decreased (A'-B': cross sectional) in CCM samples. DAPI (blue) is mapped in A-D and merged images in A'''-D'''. Bars: 20µm.

FIGURE 4. Immunostaining for occludin (green) and collagen IV (red) on two CCM and NBT samples, respectively. Different phenotypes of occludin distribution are observed. Similar to control vessels, the linear pattern of occludin staining is preserved but thinned (A: longitudinal). To some extent, occludin is arranged in a punctate pattern along cell-cell contacts (B: longitudinal). At other foci, vessels are completely unstained along the major length of their profile but show isolated, residual protein aggregates (C: cross sectional). Occludin is distributed in a linear pattern in microvessels of the adult human brain (cerebral cortex) (D and E). Basement membranes of capillaries are labeled by collagen IV-antibody (A-E). Nuclear staining with TO-PRO3 (blue) is shown in A-E. Bars: A, B and D, E 25 µm; C 10 µm.

FIGURE 5. Immunostaining for claudin-5 (green) and collagen IV (red) on two CCM specimens and NBT. In most instances, vessels appear negative for claudin-5. At some foci, claudin-5 is diffusely distributed within the tissue and not localized to intercellular contact sites (A: cross sectional). Few vessels show a punctate staining pattern (B: cross sectional). Decreased claudin-5 staining is seen along the EC cell contacts (C: cross sectional). Linear claudin-5 staining in capillaries of control NBT (D: longitudinal). Basement membranes of microvessels are labeled by collagen IV-antibody (A-D). Nuclear staining with TO-PRO3 (blue) is shown in A-C. Bars: A/D 30 µm; B/C 10 µm.

FIGURE 6. Confocal imaging of cryosections of CCM (CCM#1, CCM#6) and NBT (c#1, c#5) immunostained for GLUT-1 (green) and CD31 (red). In control vessels, GLUT-1 is distributed uniformly (C': cross/longitudinal; D': longitudinal). However, the glucose transporter 1 is massively downregulated in CCM tissue samples (A': cross sectional; B': cross/longitudinal). DAPI (blue) is mapped in A-D and merged images in A'''-D'''. Bars: 20µm.

FIGURE 7. Localization of fibronectin (green) and collagen VI as EC-marker (red: A''-B'') in CCM specimens: CCM#5 (A) and control: c#1 (B) by confocal microscopy. In vessels of the control tissue, fibronectin is distributed regularly (B': cross sectional). In CCM endothelial cells, fibronectin expression is impaired and irregular (A': cross sectional). DAPI (blue) is shown in A+B and merged images in A'''+B'''. Bars: 20 µm.

FIGURE 8. Analysis of FI of occludin, claudin-5, ZO-1 and GLUT-1 stainings in cryosections of CCMs and control tissues. Experiments were done in triplicates. (A) MFI of each CCM and control specimen; (B) MFI (in %) of the seven normalized CCM specimens versus controls. Mean control MFI was calculated as 100% (mean ± standard error of mean). Changes in MFI were calculated as highly significant for all proteins examined (students *t*-test, $p < 0.0001$, ****).

FIGURE 9. Relative mRNA expression of occludin, claudin-5, ZO-1 and GLUT-1 in CCM and NBT. Data is shown as mean values ± SEM of two individual experiments with eight samples in each group. Data were normalized against the EC-marker gene CD31. mRNA expression levels from NBT (n=8)

are set to as 100% (mean ± standard error of the mean). Differences in mRNA concentrations were determined by the Mann-Whitney-Wilcoxon test with $p < 0.05$ being considered statistically significant.

Legends to supplementary figures

FIGURE S1. Confocal imaging of paraffin sections of CCM (CCM#1) and NBT (c#1) immunostained for occludin (green) and vWF (red). In control vessels, occludin is distributed in a linear pattern (C': cross sectional; D': longitudinal). However, occludin is massively downregulated in CCM tissue samples (A' and B': cross sectional). DAPI (blue) is mapped in A-D and merged images in A'''-D'''. Bars: 20µm.

FIGURE S2. Immunostaining for GLUT-1 (green) and vWF (red) in paraffin embedded CCM and NBT specimens (CCM#3; c#1). Decreased or absent GLUT-1 staining is seen in vessels of CCM tissue (A' and B': cross sectional). In capillaries of control NBT, GLUT-1 is distributed uniformly (C': cross sectional; D': longitudinal). ECs are labelled against the marker protein vWF (A''-D''). Nuclear staining with DAPI (blue) is shown in A-D. Bars: 20 µm.

Impairment of tight junctions and glucose transport in endothelial cells of human cerebral cavernous malformations.

Hannah Schneider, Ph.D.[1,+], Mariella Errede, Ph.D.[2], Nils H. Ulrich, M.D.[1], ~~Issam A. Awad, M.D.[3], Robert Shenkar, Ph.D.[3],~~ Daniela Virgintino, M.D., Ph.D.[2], Karl Frei, Ph.D.[1], Helmut Bertalanffy, M.D.[1]

(1) Department of Neurosurgery, University Hospital, Zurich, Switzerland

(2) Department of Human Anatomy and Histology, Bari University Medical School, Italy

~~(3) University of Chicago Pritzker School of Medicine, Chicago, IL, 60637~~

(+) Hannah Schneider

phone: +41-44-2559828

fax: +41-44-2554505

email: hannah.schneider@usz.ch

Abstract

Cerebral cavernous malformations (CCMs) often cause hemorrhages which can result in severe symptoms like hemiparesis or seizures. The underlying mechanism behind the aggressive behavior of a CCM lesion is undetermined to date, but alterations of vascular matrix components may be responsible. Hence, we investigated the localization of the tight junction proteins (TJPs) occludin, claudin-5 and ZO-1 within endothelial cells. Additionally, we examined the expression of glucose transporter 1 (GLUT-1) which is sensitive to alterations in TJP levels. Seven CCM and five control (normal brain tissue) specimens were examined by fluorescent immunohistochemistry for occludin, claudin-5, ZO-1 and GLUT-1. Our p~~P~~rotein expression analysis showed that occludin, claudin-5 and ZO-1 were downregulated at intercellular contact sites and partly redistributed within the surrounding tissue in all patients examined. We also observed a massive reduction of GLUT-1 that was not observed in any of the control specimens.~~and~~ C~~c~~orresponding analysis~~mRNA levels were quantified~~ using quantitative real-time RT-PCR (qRT-PCR), revealed a ~~and analyzed using appropriate software and microarray analysis, respectively~~significant downregulation in mRNA-expression of occludin, claudin-5, ZO-1 and GLUT-1. ~~Here we show that occludin, claudin-5 and ZO-1 are downregulated at intercellular contact sites and partly redistributed within the surrounding tissue in all patients examined. These findings are accompanied by a massive reduction of GLUT-1 that was not observed in any of the control specimens. In contrast, only ZO-1 mRNA is significantly downregulated in CCM tissue suggesting a crucial role in proper TJ assembly.~~

Keywords: cerebral cavernous malformation, tight junctions, occludin, claudin-5, ZO-1, GLUT-1

Introduction

Cerebral cavernous malformations and arteriovenous malformations (AVMs) present the most common lesion subtypes of vascular malformations of the brain (VMBs), affecting more than 0.5% of the population (1-4). CCMs are composed of dilated, blood filled capillary clusters lined by endothelium, lacking intervening brain parenchyma. Due to the expression of angiogenic factors, they reflect more a developing rather than a mature vessel phenotype (1, 3, 5-7). Cavernous malformations occur sporadically, as a single lesion, or as an inherited, autosomal dominant form with multiple lesions (8). To date, mutations in three genes have been identified to cause the familial form of the disease: *CCM1/KRIT1*, *CCM2/MGC4607* and *CCM3/PDCD10* (9). It has been hypothesized that a second hit in the somatic allele is necessary to cause CCM formation. Indeed, in 2005, a biallelic *CCM1* somatic and germ line mutation has been shown in a surgically excised human lesion for the first time (10). In the meantime, biallelic mutations were also reported for *CCM2* and *CCM3* (11). Furthermore, transgenic mice heterozygous for *Ccm1*, only develop CCM lesions when they exhibit an additional homozygous knockout of the tumor suppressor gene *Trp53* ($ccm1^{+/-}$ $Trp53^{-/-}$). Similarly, heterozygous mice with $Ccm2^{\pm}$ only form CCM lesions when sensitized by a second hit (12, 13). This further supports the hypothesis of a second genetic somatic mutation in CCMs.

Recently, it was shown that CCM1 represents an antiangiogenic protein and that gene mutations in *KRIT1* correlate with excessive capillary sprouting, which is characteristic for human CCM pathology (7). PTEN promoter methylation, HEG transmembrane receptor expression, RhoA GTPase and ROCK activation are involved in the pathogenesis (14-17) and therefore have also been suggested to contribute to the mechanism of lesion formation.

Endothelial cells (ECs) are the major component of vessel walls. It is thought that they play a central role in the clinical behavior of a cerebral vascular malformation showing abnormal ultrastructural pathological features (18). The thin walls of CCM vessels possess limited number of intact interendothelial tight junctions, which may contribute to the ~~known~~ propensity of recurrent microhemorrhage seen in CCMs (19). There is growing evidence that an impairment of the blood-brain barrier (BBB) correlates with a decrease of tight junctions in the endothelial layer and

furthermore that CCM1 as well as CCM2 could play a junction stabilizing role (15, 17, 20, 21). Recently, it was shown TJP occludin to be involved in intercellular gap formation reflecting BBB breakdown in porcine brain capillary endothelial cells (22).

Tight junctions are located at the lateral apical side of the cell membrane in regions of close cell–cell contacts, e.g. in the cerebral microcapillary endothelium. They turn cell-to-cell contacts into zones of tight adherence thereby inhibiting the paracellular pathway for drugs or solutes from plasma into the central nervous system (CNS) (23). Different integral membrane proteins, associated cytoplasmatic proteins and extracellular matrix components are involved in the proper assembly of tight junction complexes (24). Two junctional core proteins, occludin and claudin-5 play a key role in BBB integrity in the microvascular endothelium. Both consist of four transmembrane domains, intracellular N- and C-termini, and two extracellular domains that might interact with cell membranes of vicinal cells thus sealing the intercellular clefts (22, 25, 26). Different gain-of-function and loss-of-function experiments reveal that claudin-5 is involved in the structure of TJ strands and cell adhesion, whereas occludin probably has some accessory functions (27). Furthermore, adaptor/scaffold proteins such as zonula occludens (ZO-1, ZO-2 and ZO-3) connect TJ-associated integral membrane proteins to the actin cytoskeleton and other structural proteins. The first reported linker protein, ZO-1 directly interacts with occludin and claudins and is essential for TJ formation (27, 28). It was hypothesized that the interaction of occludin with ZO-1 modulates its function in sealing the junction, since paracellular permeability increases when an imbalance occurs between occludin and ZO-1 molecules (29, 30).

The localization of glucose transporter 1 (GLUT-l) in ECs of microvessels is considered as an indicator of a functioning BBB (31-33). The protein is widely expressed in adult tissues, but it is most abundant in fibroblasts, erythrocytes and endothelial cells with low levels of expression in muscle, liver and adipose tissue (34-36). In healthy brain endothelium, TJ sealing of the interendothelial clefts is linked to the expression of GLUT-1. Alterations in transporter protein expression are directly related to an increased permeability of endothelial layers in the brain and also linked to alterations in TJ properties (31-33).

To date, the role of TJs and their core proteins occludin and claudin-5 are not fully understood in the context of CCM lesions. But there is growing evidence that vascular development and endothelial

permeability are dysregulated (37). In brain tumor pathology it was shown, that decreased expression of GLUT-1 is coupled to alterations in TJP expression levels and consequently BBB opening (38). Therefore, we analyzed the expression of TJPs (occludin, claudin-5 and ZO-1) and the transporter protein GLUT-1 by classic~~al~~ immunohistochemistry and confocal fluorescent microscopy on cryo- and ~~vibratome~~paraffin-sections of seven CCM specimens and five control samples (normal brain tissue; NBT). NBT specimens were received from temporal lobe biopsy during selective amygdalohippocampectomy from patients with temporal lobe epilepsy (TLE). Mean fluorescence intensity was further quantified. Furthermore, ~~Microarray analysis~~qRT-PCR was also performed to compare ~~gene~~ mRNA expression levels of TJPs and GLUT-1 ~~between~~ in eight CCM ~~and~~ versus eight control samples.

Materials and Methods

Patients and tissue specimens

~~Seven~~ Twelve CCM specimens were obtained from patients undergoing neurosurgical resection. ~~Five~~ Thirteen human control tissue specimens (NBT) were received from temporal lobe biopsy during selective amygdalohippocampectomy from patients with TLE. The median age of the ~~five~~ seven female and ~~two~~ five male patients was 3~~8~~9 (range 2~~3~~7 to 52 years). The clinical data of the ~~seven~~ twelve CCM patients is summarized in Table 2~~1~~. List of patients included in this study is based on the consensus recommendations for minimal reporting variables in CCM clinical research (39-41). ~~Indication~~ The decision for surgical resection~~ery~~ was ~~performed~~ made based on ~~after~~ computed tomography scan and magnetic resonance imaging. Tissue specimens were immediately transferred to the laboratory on ice and divided for snap-frozen preparation and *in vitro* ~~cell culture~~experiments. Samples were snap-frozen in liquid nitrogen (NO_2) and embedded in TissueTek O.C.T (Satura Finetek Europe, Zoeterwoude, Netherlands) before analysis. Additionally, histological diagnosis was obtained by routine clinical neuropathological examination and classified according to the World Health Organization standards (Institute of Neuropathology, University Hospital Zurich, Switzerland).

Immunofluorescence, laser scanning confocal microscopy and fluorescence microscopy analysis

Immunofluorescence analysis was done by three~~wo~~ different protocols. First, 6 µm cryosections were cut with a Leica cryostat, mounted on Superfrost®Plus slides (Menzel-Glaser, Braunschweig, Germany), fixed with acetone p.a~~A~~. for 10 min at room temperature (RT) and stored at -80°C till further use. For analysis, slides were acetone-fixed for 5 min at RT and air-dried. Sections were incubated with 3% peroxide to quench endogenous peroxidase activity and washed with PBS (pH 7.4). Unspecific binding sites were blocked with blocking solution (Candor, Weißensberg, Germany) for 25 min at RT. For indirect immunofluorescence, polyclonal rabbit anti-human claudin-5-antibody (5 µg/ml; Abcam, Cambridge, UK), ~~polyclonal~~ monoclonal mouse~~rabbit~~ anti-human occludin-antibody (4 µg/ml; Invitrogen, Carlsbad, CA ~~CA,~~ USA), monoclonal mouse anti-human GLUT-1-antibody (1 µg/ml; Abcam, Cambridge, UK), monoclonal mouse anti-human fibronectin (2 µg/ml; Abcam,

Cambridge, UK), mouse monoclonal anti-human CD31 (10µg/ml; DAKO, Glostrup, DK), monoclonal rabbit anti-human CD31 (1:40; epitomics, Burlingame, CA, USA), ~~and~~ monoclonal mouse anti-human collagen-IV-antibody (2 µg/ml; DAKO, Glostrup, DK) and polyclonal rabbit anti-human collagen-VI-antibody (2 µg/ml; Abcam, Cambridge, UK) were incubated at 37°C for 1h. Appropriate secondary antibodies, ALEXA 488-conjugated (goat anti-rabbit and goat anti-mouse 1:100, Invitrogen, Carlsbad, CA, USA) or ALEXA 594-conjugated secondary antibody antibody (goat anti-rabbit and goat anti-mouse, 1:100, Invitrogen Carlsbad, CA, USA) were incubated for 25 min at RT. All antibodies were diluted in "~~Antikörper Verdünnungspuffer~~Antibody Dilution Buffer" (DCS, Hamburg, Germany). Between each step, the sections were washed in PBS three times 5 min each. Control stainings~~s~~ included the isotype matched primary monoclonal antibodies. In all cases, the result~~s~~ of ~~the~~ each negative control~~s~~ confirmed the specificity of the corresponding antibody staining. Specimens were mounted in fluorescent mounting medium (DAKO, Glostrup, DK) and sections were viewed on a Leica TCS SP5 (Leica, Wetzlar, Germany) confocal laser scanning microscope (CLSM) using 63x and 100x objectives. Confocal images were taken at 1-2 µm intervals through the z-axis of the section. Projection images formed by serial optical planes were analyzed, digitally recorded, and stored as tagged image file f~~F~~ormat files using Adobe Photoshop CS3 software (Adobe Systems, San Jose, CA, USA). Second, tissue samples were placed into 4% neutral buffered formalin for twelve hours, and then were processed routinely for paraffin inclusion. Sections were obtained at 4 µm intervals using a Microm rotary microtome (Leica, Wetzlar, Germany), put in water and mounted to Superfrost®Plus slides (Menzel-Glaser, Braunschweig, Germany). After rehydration, for antigen retrieval, sections were boiled in a microwave oven in 0.01M citrate buffer solution (pH 6) for 20 minutes. Endogenous peroxidase was inactivated with 3% hydrogen peroxide and nonspecific antigenic sites were blocked with blocking solution (Candor, Weißensberg, Germany) for 25 minutes at RT. As already described above, sections were incubated with primary occludin- (4 µg/ml, Invitrogen, Carlsbad, CA, USA), GLUT-1- (1 µg/ml; Abcam, Cambridge, UK) and polyclonal rabbit anti-human vWF-antibodies (28.5 µg/ml; DAKO, Glostrup, DK) followed by incubation with appropriate secondary antibodies, ALEXA 488-conjugated (goat anti-mouse 1:100, Invitrogen, Carlsbad, CA, USA) or ALEXA 594-conjugated secondary antibody antibody (goat anti-rabbit, 1:100,

Invitrogen, Carlsbad, CA, USA). Third, tissue specimens were fixed for 3 h at 4°C by immersion in 2% paraformaldehyde plus 0.2% glutaraldehyde solution and washed in PBS (pH 7.6). The blocks of tissue were sectioned at 20 µm thickness using a vibrating microtome (Leica, Wetzlar, Germany ~~Microsystem; Milan, Italy~~) and sections were collected on polylysine slides (Menzel-Glaser, Braunschweig, Germnay~~, GmbH~~). Heat-mediated antigen retrieval was achieved by microwave pre-treatment in 0.01 M citrate buffer (pH 6.0) for 15 min at 750W. Sections were incubated with PBS/0.5% Triton X-100 for 30 min, blocked with protein block serum free (DAKO, Glostrup, DK) for 15 min at RT and incubated overnight at 4 °C with primary antibodies at various dilutions: mouse monoclonal anti-human claudin-5 (1:20; Zymed Laboratories, Invitrogen, Carlsbad, CA, USA), rabbit polyclonal anti-human occludin (1:50; Zymed Laboratories, Invitrogen, Carlsbad, CA, USA), rabbit polyclonal anti-human collagen IV (1:200; Acris Antibodies GmbH, Hiddenhausen, Germany), mouse monoclonal anti-human collagen IV (1:50; DAKO, Glostrup, DK) and mouse monoclonal anti-human CD31 (1:50; DAKO, Glostrup, DK). A mixture of biotinylated horse anti-mouse (1:400; Vector, Vector Laboratories, Inc.; Burlingame, CA, USA) or biotinylated goat anti-rabbit IgG (1:400; Vector, Vector Laboratories, Inc.; Burlingame, CA, USA) and Alexa568-conjugated goat anti-rabbit (1:400, Invitrogen, Carlsbad, CA, USA) or Alexa555-conjugated goat anti-mouse IgG (1:400, Invitrogen, Carlsbad, CA, USA) were incubated as secondary antibodies for 40 min at RT. Streptavidin Alexa Fuor 488-conjugated (1:400; Invitrogen, Carlsbad, CA, USA) was used for staining of claudin-5 and occludin. The slices were counterstained with TO-PRO-3 (1:10.000 in PBS; Invitrogen, Carlsbad, CA, USA) and finally mounted with Vectashield (Vector Vector Laboratories, Inc.; Burlingame, CA, USA) and sealed with nail varnish. The stainings were examined under the Leica TCS SP5 confocal laser scanning microscope (Leica, Wetzlar, Germany ~~Microsystems~~) using a sequential scan procedure during image acquisition of double-labeled sections. Confocal images were taken at 250-500 nm intervals through the z-axis of the sections. Images from individual optical planes and image projections of stacks of serial optical planes were analyzed by Leica confocal software (Multicolor Package; Leica, Wetzlar, Germany ~~Microsystems~~).

Image Acquisition, image processing and data analysis

Digital image processing for the detection and quantification of fluorescent intensitiy (QFI) in human CCM and control samples was performed with a conventional light microscope (Axiovert 100, Zeiss, Jena, Germany), a digital microscope camera (AxioCam ICm, Zeiss, Jena, Germany) and the AxioVision 4.8 software (Zeiss, Jena, Germany). Fluorescence quantification was sub-divided into image acquisition, image preprocessing, and data processing steps (42). All parameters used in the acquisition were standardized (detector gain, exposure time) to maintain high reproducibility. Image processing of each specimen was provided through region of interest (ROI) analysis. The software allows the interactive definition of areas for size and intensity measurements. For data analysis, fluorescence intensity/ROI values were obtained for five ROIs/specimen (10 μm^2 each). Statistical analysis describing the distribution of the intensity of the fluorescence signals was performed to obtain graphical representations.

Quantitative RT-PCR analysis

Differential gene expression levels of claudin-5, occludin, ZO-1 and GLUT-1 were determined by q RT-PCR. Therefore, total RNA was isolated from each cavernoma and control tissue sample using the RNeasy Mini Kit Isolation System according to the manufactor's protocol for RNA extraction (Qiagen Ltd., Hombrechtikon, Schweiz). 0.5 µg total mRNA of each sample was reverse transcribed to cDNA using the High Capacity cDNA Reverse Transcription Kit (ABI, Carlsbad, CA, USA). cDNA was used for qRT-PCR with SYBR® Green PCR Master Mix (ABI, Carlsbad, CA, USA) and specific primer pairs on a 7900HT Fast Real-Time PCR System with SDS Software v2.4 (ABI, Carlsbad, CA, USA). Expression was normalized against the endothelial marker CD31 or vWF. Specific primers were designed with the Primer Express 3.0 software (ABI, Carlsbad, CA, USA) and are listed in Table 1.

~~**Gene expression analysis**~~

~~Differential expression of occludin, claudin-5, ZO-1 and GLUT-1 genes was analyzed by microarray as previously described in Shenkar et al. (43). A total of 9 specimens including 6 CCMs (CCM#10-15) and 3 normal vessels (superficial temporal arteries (STAs), STA#1-3) were obtained from patients~~

~~between 2000 and 2003 and the study was approved by the IRB of the University of Colorado (COMIRB). The median age of the five female and one male patient was 28 (range 9 to 40 years). The relevant clinical and lesion features of the cases are listed in Table 2.~~

Statistical analysis

For quantification and statistical analysis of protein expression levels, experiments were done in triplicates analyzing five ROIs/specimen (10µm^2) for each patient. Mean fluorescence intensity (MFI) values were calculated and averaged. ROIs were selected randomly by criteria that only fluorescent signals of vessel wall structures were measured for their intensity. The statistical analysis, using the mean fluorescence intensity values of each patient, was performed with Microsoft Excel and GraphPad Prism software (version 5 for Windows). To assess whether two independent samples of observations come from the same distribution, an unpaired students *t*-test was used. P-values < 0.01 were considered as statistically significant.

mRNA expression levels of each gene were obtained via correction for endothelial density. The results are expressed as means ± standard error (SEM). Statistical evaluation was performed with GraphPad Prism software (version 5 for Windows). Statistical significance was determined by Mann-Whitney-Wilcoxon Test . ~~Therefore, values (CCM versus STA) were calculated by dividing the expression level of genes of interest (TJPs and GLUT-1) by the expression levels of the EC marker protein CD105 (endoglin). Subsequently, values were normalized on the particular mean value of STA specimens.~~ P-values < 0.05 were considered as statistically significant.

Results

Comparison of TJPs between CCM and NBT microvessels

Initially, protein expression patterns of TJPs occludin, claudin-5 and ZO-1 from seven CCM and five control specimens were examined on intact vascular structures by fluorescent immunohistochemistry and analyzed via laser scanning confocal microscopy (representative images of following samples are shown: Fig. 1: CCM#1, CCM#2, c#2 and c#4; Fig. 2: CCM#2,CCM#3, c#2 and c#4; Fig. 3: CCM#2, CCM#3, c#1 and c#4 and Fig. S1: CCM#1, c#1 and Fig. 4: CCM#1, CCM#6, c#1 and c#5). The levels of the TJP expressions were compared to control tissues obtained from patients with temporal lobe epilepsy who had undergone surgery. Representative results for two CCM and control specimens, respectively, are shown in Ffigs. 1-3 and S14. To identify endothelial cells (ECs), sections were co-stained for the EC marker protein PECAM-1/CD31 on cryosections (Fig.1-34: A''-D'' and A'''-D''') and von Willebrand factor (vWF) on paraffin sections (Fig. S1: A''-D''). In the endothelial layers of CCM tissue, Pprotein expression of occludin, claudin-5 and ZO-1 was clearly decreased in endothelial layers of CCM tissue , compared to control brain microvessels, which showed a typical linear staining pattern at distinct endothelial cell borders. The linear junctional labeling was either discontinuous or amorphous and many vessels even appeared negative for TJPs. In several cases, redistribution of proteins was observed in the endothelial layer as well as the surrounding tissue (Fig. 1-3: A'-C'). Co-staining for CD31 and vWF additionally revealed that only microvessels were analyzed for impairment in TJP localization.

We then proceeded to build three dimensional reconstructions of vascular structures to validate the immunofluorescence experiments which showed different localization patterns for TJPs along the margin of cell–cell contacts and in the surrounding tissue of CCMs when compared to controls (Fig. 45 and 56). In CCM tissue, in regions where a protein signal could be determined, few vessels showed a punctuate labelling for claudin-5 (Fig. 4B/C and 56A/B), in others occludin and claudin-5 were linearly arranged along the endothelial cell-cell contacts as it was observed in the vessels of control tissues (Fig. 45A; Fig. 56C). In those cases, the fluorescence signal of both proteins was clearly weakened compared to the signal intensity in healthy tissue. Furthermore, in vessels of control tissues,

occludin and claudin-5 staining was limited to the vascular intima (Fig. 4~~5~~D/E and 5~~6~~D), whereas it could also be detected in the surrounding tissue in some regions of the CCM sections (Fig. 5~~6~~A).

GLUT-1 expression in CCM vessels

Alterations in transporter protein expression are directly related to an increased permeability of endothelial layers in the brain and also linked to alterations in TJ properties (31-33).

To investigate BBB permeability, which not only corresponds to alterations in TJPs but to an impairment of GLUT-1 expression, we also stained CCM and control tissue cryosections for thise transmembrane transporter protein (shown in Fig. 6 for samples: CCM#1, CCM#6, c#1 and c#5 on cryosections and Fig. S2: CCM#3, c#1 on paraffin embedded sections). We could observe that microvessels of control brain tissues were stained uniformly and showed a high level of GLUT-1 expression (Fig. 6 and S2: 4C'-D'). Unlike in controls, GLUT-1 expression was reduced or ~~altogehter~~absent in CCM specimens (Fig. 6 and S2: 4A'-B'). As an internal positive control, erythrocytes were stained in every sample, to reflect membranous GLUT-1 activity (Fig. 6 and S2: B'). To conclude, linear TJP localization at EC boarders was clearly disrupted and accompanied by a massive reduction of GLUT-1 staining. This reflects an impairment of the BBB, which is supported by vessel leakage illustrated in Fig. 7 by an irregular fibronectin staining around CCM microvessels. ~~As an internal positive control, erythrocytes were stained in every sample, to reflect membranous GLUT-1 activity (Fig. 4B''-C'').~~

Alterations in TJP and GLUT-1 expression in CCMs

For further analysis, alterations in protein expression levels were quantified by determining signal intensities of immunofluorescent labeled cryosections of CCM against the intensities in control specimens. As described above, a strong reduction of TJP and ~~glucose transporter protein~~GLUT-1 levels were observed along EC cell borders, corresponding to decreased FI per ROI (Fig. 8~~7~~). A drop of occludin-, claudin-5-, ZO-1- and GLUT-1-fluorescence signal was determined in each CCM specimen (Fig. 8~~7~~A). Slight differences in the extent of protein reduction are due to unique tissue composition of each CCM sample. Mean values, calculated for CCMs and controls, revealed a FI

signal reduction of 62% for occludin, 71% for claudin-5 and 74% for ZO-1 in CCM tissue compared to those in control tissue (Fig. 87B). The decrease of fluorescence intensity/protein expression in CCM vessels was found to be highly significant in all cases ($p < 0.0001$, ****).

Hence, the most striking decrease of protein expression in pathologic vessels was found for GLUT-1 (78%). Again, reduction was determined as highly significant by an unpaired students *t*-test ($p < 0.0001$, ****).

mRNA expression ~~Microarray~~ analysis of ~~TJP~~ occludin, claudin-5, ZO-1 and GLUT-1 ~~gene expression between~~ in CCM~~s and STAs~~

As shown above, protein levels of TJPs occludin, claudin-5, ZO-1 and glucose transporter GLUT-1 are downregulated at intercellular contact sites and in microvessels of CCMs, respectively. In order to validate those findings, we performed real-time RT-PCR and normalized against either endothelial marker CD31 (Fig. 9) or vWF (not shown), showing similar results. T~~t~~otal RNAs from eight~~six~~ samples were analyzed for each group (CCM and ~~three~~ NBT)~~STA samples were analyzed using a gene discovery approach and the confirmation of known gene methodologies described in Shenkar et al. (43). In our study, TJ and GLUT-1 protein levels were found to be downregulated at intercellular contact sites and in microvessel plasma membranes, respectively, in CCM specimens. Thus, microarray analysis was performed to determine relative mRNA expression levels for the genes of interest. Subsequently, values were divided by the mean of relative mRNA expression levels of the EC marker genes CD31 (PECAM-1), CD105 (endoglin), CD146 (MCAM) and Von Willebrand factor (vWF) (Fig. 8). This was done to correct variations in tissue compositions (EC density) among specimens. Interestingly, relative amounts of occludin, claudin-5, ZO-1 and GLUT-1 mRNA were not significantly altered in CCM samples compared to STAs (students *t*-test, $p > 0.05$)~~RN. A expression of occludin (13±3.6%), claudin-5 (25.8±8.3%) and ZO-1 (8.2±3.6%) was significantly decreased in CCM versus to NBT samples (Mann-Whitney-Wilcoxon-Test, $p < 0.05$)~~There was a slight trend for an increase in occludin ($p = 0.1846$) and claudin-5 ($p = 0.2133$) gene expression levels in CCMs. Moreover, weaker tendency of ZO-1 gene expression was observed in CCMs compared to levels in

~~STAs (p = 0.1896). Finally, no alterations in GLUT-1 mRNA levels were found in CCMs versus controls (p = 0.8264).~~

:

Similarly, GLUT-1 was also significantly reduced (15.8±4.3) when compared with RNA expression in NBT.

Discussion

In this study, we discovered that tight junction proteins occludin, claudin-5, ZO-1, and glucose transporter protein GLUT-1 compositions are impaired in CCM tissue. Expression of these proteins was strongly reduced at interendothelial contact sites, and appeared negative in most of the vessels.

In healthy endothelial layers, correct assembly of TJs is essential for the maintenance of a functional permeability barrier. It is known, that the structural composition of TJs in ECs of brain capillaries is the most complex among any other physiological systems (43). Therefore, it is suggested that an impairment of TJ assembly can lead to a loss of BBB integrity (44-46). Furthermore, localization of GLUT-1 is considered to be an excellent indicator of a normally functioning BBB (31-33). We therefore investigated the expression of TJPs and GLUT-1 to get more information about subcellular events leading to an aggressive behavior of a CCM lesion. In fact, occludin and claudin-5, which are critical for proper BBB function and permeability (45, 47, 48), are downregulated at interendothelial contact sites in CCM tissue. Furthermore, we observed that TJ-associated protein ZO-1 expression was also altered. ZO-1 and occludin are considered to be the most important protein components for the maintenance of the barrier function of brain microvessels (49-51). Additionally, previous studies have found occludin to play an important role in the regulation of brain capillary permeability (52). Other studies show that claudin-5 plays an essential role in TJ formation generating the structural and functional core of the multiprotein complex (27). Our findings, of deviations in TJP localization, are accompanied by clear protein redistribution within the surrounding brain parenchyma of CCM vessels. The resulting incorrect assembly of TJs may lead to a malfunction of proper BBB. Moreover, downregulation of ZO-1 suggests a disturbance in interaction of TJs with the actin cytoskeleton, strongly assuming a direct influence in the pathology of CCMs. This may lead to the possibility of a disruption in the cellular architecture, which may consequently lead to decreasing cellular stability. It is known, that downregulation of ZO-1 in CCMs results in a mismatch between interacting TJPs. Furthermore, overexpression of occludin and inadequate levels of ZO-1 enhance the impairment of the BBB (29). Additionally, occludin phosphorylation correlates with TJ formation and regulation of junction permeability and interaction with ZO-1 (53-55). As claudin-5 is a key determinant of trans-

endothelial resistance at the BBB, alterations in its interacting proteins can also lead to a disruption of the barrier function (53).

Taken together, our observations give strong evidence that cell-cell contacts of CCM vessels are disorganized to some extent and that TJ proteins are redistributed in parts of the EC surrounding tissue. These observations suggest an alteration of tight junction assembly in CCMs leading to a malfunctioning permeability barrier, like it is reported in brain tumor vessels or in brain microcapillaries after ischemic events (22, 38, 56). And indeed, in many patients, CCM pathology comprises repeated microhemorrhages into the surrounding brain parenchyma corresponding to an impaired permeability of brain capillaries. Recently, it was shown in a CCM mouse model, that heterozygosity at *Ccm2* locus impaired endothelial barrier function via alterations in cell-to-cell interactions, cytoskeletal architecture and lumen formation (15). In addition, loss of CCM1 results in disruption of junctional stability that leads to increased permeability *in vitro* and *in vivo*. It also has been shown that the activation of the Rho GTPase RhoA and its downstream effector ROCK, in turn, caused by a loss of CCM1 and CCM2, influences vascular leakage (15, 17). Therefore, most likely either direct and linker protein mediated interactions between CCM1/CCM2 and TJPs probably exist.

However, it has to be mentioned, that CCM vessels are not devoid of correctly assembled TJ complexes, even though expression was weakened, linear staining patterns of occludin, claudin-5 and ZO-1 could still be observed along the endothelial cell-cell contacts in very few CCM foci. Therefore, further examinations must be carried out to investigate whether higher percentage of linear TJP arrangement at cell-cell-boarders correlates with the aggressive clinical behavior of a lesion, as already suggested by other groups (20, 57).

Quantification of signal intensities of TJP expression confirmed our initial immunohistochemical observation. Downregulation of occludin, claudin-5 and ZO-1 in regions of interendothelial contact sites has been shown to be highly significant and strongly validates the assumption that TJP are critical for the barrier function of brain vasculature and thus disruption of their expression leads to an impairment of BBB function.

We also investigated the expression pattern of GLUT-1 within CCMs, since it was shown that alterations of TJP was paralleled by a reduction of GLUT-1 in cerebral endothelial cells and is

consistent with BBB opening in tumor tissues (31-33, 38). Furthermore, it is known, that BBB breakdown occurs in human CCMs and is, amongst others, thought to be responsible for ~~an~~ aggressive behavior of a lesion (20, 57). However, an underlying mechanism leading to an expansion and rupture of a CCM lesion, remains a mystery (58). As already expected, alterations in TJP distribution was accompanied by a massive downregulation of GLUT-1, which is found to be highly significant. This effect was accompanied by an irregular fibronectin staining which reflects vessel leakage. In most CCM vessels, GLUT-1 is completely absent and with positive signal being detectable in erythrocytes only. Staining of red blood cells in extravascular CCM tissue either indicates recent hemorrhage and serves as an internal positive control. GLUT-1 is the only known endothelial BBB glucose transporter protein, therefore its downregulation is probably correlated to impaired glucose uptake into the brain and metabolic rate of cells (59).

Our analysis revealed that ~~alterations~~ the scarcity of in TJP and GLUT-1 protein ~~distribution~~ levels did ~~not~~ correspond to modifications in gene expression. Changes in relative amounts of TJP- and GLUT-1-mRNA were evaluated as ~~not~~highly ~~statistically~~ significant. Therefore it appears to be obvious that differences in protein concentrations at TJs and EC plasma membranes are caused by downregulation of mRNA expression. Additionally, to some extent, impaired ~~posttranscriptional and posttranslational events, respectively. It also substantiates suspicion that~~ impaired ~~alterations in~~ TJP and GLUT-1 levels in CCM vessels may also correspond to protein redistribution within the tissue which could be influenced by alterations with further binding partners. In this context, impaired interactions with adherens junction components (AJs) could also play a role. The most important element of AJs consists of the VE-Cadherin/β-catenin complex (60). It is known, that CCM1/Krit1 interacts with β-catenin, which in turn shows cross-reaction with TJs, probably in a Rap-1 GTPase-dependent manner (21, 61). Therefore it should be taken into account that alterations in TJPs and GLUT-1 levels could in turn influence or be caused by impairments in AJ protein components.

~~, instead of downregulation at absolute protein expression levels.~~

In conclusion, our data strongly supports the fundamental role of TJ complexes and TJP in the pathogenesis of CCMs. We were able to show that CCM pathology corresponds to an impaired localization of occludin, claudin-5 and ZO-1 at interendothelial contact sites, which is accompanied by

a massive reduction of GLUT-1 in dilated CCM microvessels. These findings may affect vascular matrix stability, and thus can contribute to an aggressive clinical behavior seen in CCMs. Future attempts will need to study the interactions of TJPs with *CCM1, 2* and *3* gene products and other binding partners, for example AJ proteins. Furthermore, more information about the role of TJPs in the formation of a tight BBB in CCM will greatly facilitate a better understanding of lesional behavior and could be beneficial in the development of an appropriate treatment.

Acknowledgments

This research was supported by the Center for Clinical Research at the University of Zurich. The authors thank the Center for Microscopy and Image Analysis, University of Zurich, for the use of the CLSM and technical assistance. The authors thank Mushfika Ahmad (Departments of Neurosurgery and Neurology, University Hospital, Zurich) for meticulous editorial revision and Dr. Johannes Schmitt and Claudia Gottier (Division of Gastroenterology and Hepatology, University Hospital Zurich) for their assistance in RT-PCR performance.

Conflict of interest

The authors declare that they have no conflict of interest.

References

1. Al-Shahi R, Bhattacharya JJ, Currie DG, Papanastassiou V, Ritchie V, Roberts RC, Sellar RJ, Warlow CP. Prospective, population-based detection of intracranial vascular malformations in adults: the Scottish Intracranial Vascular Malformation Study (SIVMS). Stroke 2003e:34;1163-9.

2. Del Curling O, Jr., Kelly DL, Jr., Elster AD, Craven TE. An analysis of the natural history of cavernous angiomas. J Neurosurg 1991e:75;702-8.

3. Rigamonti D, Hadley MN, Drayer BP, Johnson PC, Hoenig-Rigamonti K, Knight JT, Spetzler RF. Cerebral cavernous malformations. Incidence and familial occurrence. N Engl J Med 1988e:319;343-7.

4. Leblanc GG, Golanov E, Awad IA, Young WL. Biology of vascular malformations of the brain. Stroke 2009e:40;e694-702.

5. Rothbart D, Awad IA, Lee J, Kim J, Harbaugh R, Criscuolo GR. Expression of angiogenic factors and structural proteins in central nervous system vascular malformations. Neurosurgery 1996e:38;915-24; discussion 24-5.

6. Kilic T, Pamir MN, Kullu S, Eren F, Ozek MM, Black PM. Expression of structural proteins and angiogenic factors in cerebrovascular anomalies. Neurosurgery 2000e:46;1179-91; discussion 91-2.

7. Wustehube J, Bartol A, Liebler SS, Brutsch R, Zhu Y, Felbor U, Sure U, Augustin HG, Fischer A. From the Cover: Cerebral cavernous malformation protein CCM1 inhibits sprouting angiogenesis by activating DELTA-NOTCH signaling. Proc Natl Acad Sci U S A 2010e:107;12640-5.

8. Mindea SA, Yang BP, Shenkar R, Bendok B, Batjer HH, Awad IA. Cerebral cavernous malformations: clinical insights from genetic studies. Neurosurg Focus 2006e:21;e1.

9. Labauge P, Denier C, Bergametti F, Tournier-Lasserve E. Genetics of cavernous angiomas. Lancet Neurol 2007e:6;237-44.

10. Gault J, Shenkar R, Recksiek P, Awad IA. Biallelic somatic and germ line CCM1 truncating mutations in a cerebral cavernous malformation lesion. Stroke 2005e:36;872-4.

11. Akers AL, Johnson E, Steinberg GK, Zabramski JM, Marchuk DA. Biallelic somatic and germline mutations in cerebral cavernous malformations (CCMs): evidence for a two-hit mechanism of CCM pathogenesis. Hum Mol Genet 2009e:18;919-30.

12. Shenkar R, Venkatasubramanian PN, Wyrwicz AM, Zhao JC, Shi C, Akers A, Marchuk DA, Awad IA. Advanced magnetic resonance imaging of cerebral cavernous malformations: part II. Imaging of lesions in murine models. Neurosurgery 2008e:63;790-7; discussion 7-8.

13. Plummer NW, Gallione CJ, Srinivasan S, Zawistowski JS, Louis DN, Marchuk DA. Loss of p53 sensitizes mice with a mutation in Ccm1 (KRIT1) to development of cerebral vascular malformations. Am J Pathol 2004e:165;1509-18.

14. Kleaveland B, Zheng X, Liu JJ, Blum Y, Tung JJ, Zou Z, Sweeney SM, Chen M, Guo L, Lu MM, Zhou D, Kitajewski J, Affolter M, Ginsberg MH, Kahn ML. Regulation of cardiovascular development and integrity by the heart of glass-cerebral cavernous malformation protein pathway. Nat Med 2009e:15;169-76.

15. Whitehead KJ, Chan AC, Navankasattusas S, Koh W, London NR, Ling J, Mayo AH, Drakos SG, Jones CA, Zhu W, Marchuk DA, Davis GE, Li DY. The cerebral cavernous malformation signaling pathway promotes vascular integrity via Rho GTPases. Nat Med 2009e:15;177-84.

16. Zhu Y, Wloch A, Wu Q, Peters C, Pagenstecher A, Bertalanffy H, Sure U. Involvement of PTEN promoter methylation in cerebral cavernous malformations. Stroke 2009e:40;820-6.

17. Stockton RA, Shenkar R, Awad IA, Ginsberg MH. Cerebral cavernous malformations proteins inhibit Rho kinase to stabilize vascular integrity. J Exp Med 2010e:207;881-96.

18. Zhao Y, Tan YZ, Zhou LF, Wang HJ, Mao Y. Morphological observation and in vitro angiogenesis assay of endothelial cells isolated from human cerebral cavernous malformations. Stroke 2007e:38;1313-9.

19. Wong JH, Awad IA, Kim JH. Ultrastructural pathological features of cerebrovascular malformations: a preliminary report. Neurosurgery 2000e:46;1454-9.

20. Clatterbuck RE, Eberhart CG, Crain BJ, Rigamonti D. Ultrastructural and immunocytochemical evidence that an incompetent blood-brain barrier is related to the pathophysiology of cavernous malformations. J Neurol Neurosurg Psychiatry 2001e:71;188-92.

21. Glading A, Han J, Stockton RA, Ginsberg MH. KRIT-1/CCM1 is a Rap1 effector that regulates endothelial cell cell junctions. J Cell Biol 2007e:179;247-54.

22. Lischper M, Beuck S, Thanabalasundaram G, Pieper C, Galla HJ. Metalloproteinase mediated occludin cleavage in the cerebral microcapillary endothelium under pathological conditions. Brain Res 2010e:1326;114-27.

23. Cornford EM, Hyman S. Localization of brain endothelial luminal and abluminal transporters with immunogold electron microscopy. NeuroRx 2005e:2;27-43.

24. Rosenberg GA, Yang Y. Vasogenic edema due to tight junction disruption by matrix metalloproteinases in cerebral ischemia. Neurosurg Focus 2007e:22;E4.

25. Anderson JM, Van Itallie CM. Tight junctions and the molecular basis for regulation of paracellular permeability. Am J Physiol 1995e:269;G467-75.

26. Tsukita S, Furuse M. Occludin and claudins in tight-junction strands: leading or supporting players? Trends Cell Biol 1999e:9;268-73.

27. Furuse M. Molecular basis of the core structure of tight junctions. Cold Spring Harb Perspect Biol 2010e:2;a002907.

28. Fanning AS, Jameson BJ, Jesaitis LA, Anderson JM. The tight junction protein ZO-1 establishes a link between the transmembrane protein occludin and the actin cytoskeleton. J Biol Chem 1998e:273;29745-53.

29. Feldman GJ, Mullin JM, Ryan MP. Occludin: structure, function and regulation. Adv Drug Deliv Rev 2005e:57;883-917.

30. McCarthy KM, Skare IB, Stankewich MC, Furuse M, Tsukita S, Rogers RA, Lynch RD, Schneeberger EE. Occludin is a functional component of the tight junction. J Cell Sci 1996e:109 (Pt 9);2287-98.

31. Dobrogowska DH, Vorbrodt AW. Quantitative immunocytochemical study of blood-brain barrier glucose transporter (GLUT-1) in four regions of mouse brain. J Histochem Cytochem 1999e:47;1021-30.

32. Gerhart DZ, LeVasseur RJ, Broderius MA, Drewes LR. Glucose transporter localization in brain using light and electron immunocytochemistry. J Neurosci Res 1989e:22;464-72.

33. Lippoldt A, Kniesel U, Liebner S, Kalbacher H, Kirsch T, Wolburg H, Haller H. Structural alterations of tight junctions are associated with loss of polarity in stroke-prone spontaneously hypertensive rat blood-brain barrier endothelial cells. Brain Res 2000e:885;251-61.

34. Birnbaum MJ, Haspel HC, Rosen OM. Cloning and characterization of a cDNA encoding the rat brain glucose-transporter protein. Proc Natl Acad Sci U S A 1986e:83;5784-8.

35. Fukumoto H, Seino S, Imura H, Seino Y, Eddy RL, Fukushima Y, Byers MG, Shows TB, Bell GI. Sequence, tissue distribution, and chromosomal localization of mRNA encoding a human glucose transporter-like protein. Proc Natl Acad Sci U S A 1988e:85;5434-8.

36. Pardridge WM, Boado RJ, Farrell CR. Brain-type glucose transporter (GLUT-1) is selectively localized to the blood-brain barrier. Studies with quantitative western blotting and in situ hybridization. J Biol Chem 1990e:265;18035-40.

37. Yadla S, Jabbour PM, Shenkar R, Shi C, Campbell PG, Awad IA. Cerebral cavernous malformations as a disease of vascular permeability: from bench to bedside with caution. Neurosurg Focus 2010e:29;E4.

38. Ishihara H, Kubota H, Lindberg RL, Leppert D, Gloor SM, Errede M, Virgintino D, Fontana A, Yonekawa Y, Frei K. Endothelial cell barrier impairment induced by glioblastomas and transforming growth factor beta2 involves matrix metalloproteinases and tight junction proteins. J Neuropathol Exp Neurol 2008e:67;435-48.

39. Al-Shahi Salman R, Berg MJ, Morrison L, Awad IA. Hemorrhage from cavernous malformations of the brain: definition and reporting standards. Angioma Alliance Scientific Advisory Board. Stroke 2008e:39;3222-30.

40. Kivelev J, Niemela M, Kivisaari R, Dashti R, Laakso A, Hernesniemi J. Long-term outcome of patients with multiple cerebral cavernous malformations. Neurosurgery 2009e:65;450-5; discussion 5.

41. van Swieten JC, Koudstaal PJ, Visser MC, Schouten HJ, van Gijn J. Interobserver agreement for the assessment of handicap in stroke patients. Stroke 1988e:19;604-7.

42. Di Iorio E, Barbaro V, Ferrari S, Ortolani C, De Luca M, Pellegrini G. Q-FIHC: quantification of fluorescence immunohistochemistry to analyse p63 isoforms and cell cycle phases in human limbal stem cells. Microsc Res Tech 2006e:69;983-91.

43. Nagy Z, Peters H, Huttner I. Fracture faces of cell junctions in cerebral endothelium during normal and hyperosmotic conditions. Lab Invest 1984e:50;313-22.

44. Furuse M, Hirase T, Itoh M, Nagafuchi A, Yonemura S, Tsukita S. Occludin: a novel integral membrane protein localizing at tight junctions. J Cell Biol 1993e:123;1777-88.

45. Nitta T, Hata M, Gotoh S, Seo Y, Sasaki H, Hashimoto N, Furuse M, Tsukita S. Size-selective loosening of the blood-brain barrier in claudin-5-deficient mice. J Cell Biol 2003e:161;653-60.

46. Ohtsuki S, Sato S, Yamaguchi H, Kamoi M, Asashima T, Terasaki T. Exogenous expression of claudin-5 induces barrier properties in cultured rat brain capillary endothelial cells. J Cell Physiol 2007e:210;81-6.

47. Harhaj NS, Antonetti DA. Regulation of tight junctions and loss of barrier function in pathophysiology. Int J Biochem Cell Biol 2004e:36;1206-37.

48. Hawkins BT, Davis TP. The blood-brain barrier/neurovascular unit in health and disease. Pharmacol Rev 2005e:57;173-85.

49. Bolton SJ, Anthony DC, Perry VH. Loss of the tight junction proteins occludin and zonula occludens-1 from cerebral vascular endothelium during neutrophil-induced blood-brain barrier breakdown in vivo. Neuroscience 1998e:86;1245-57.

50. Citi S. The molecular organization of tight junctions. J Cell Biol 1993e:121;485-9.

51. Vorbrodt AW, Dobrogowska DH, Tarnawski M. Immunogold study of interendothelial junction-associated and glucose transporter proteins during postnatal maturation of the mouse blood-brain barrier. J Neurocytol 2001e:30;705-16.

52. Forster C. Tight junctions and the modulation of barrier function in disease. Histochem Cell Biol 2008e:130;55-70.

53. Argaw AT, Gurfein BT, Zhang Y, Zameer A, John GR. VEGF-mediated disruption of endothelial CLN-5 promotes blood-brain barrier breakdown. Proc Natl Acad Sci U S A 2009e:106;1977-82.

54. Kebir H, Kreymborg K, Ifergan I, Dodelet-Devillers A, Cayrol R, Bernard M, Giuliani F, Arbour N, Becher B, Prat A. Human TH17 lymphocytes promote blood-brain barrier disruption and central nervous system inflammation. Nat Med 2007e:13;1173-5.

55. Sakakibara A, Furuse M, Saitou M, Ando-Akatsuka Y, Tsukita S. Possible involvement of phosphorylation of occludin in tight junction formation. J Cell Biol 1997e:137;1393-401.

56. Wachtel M, Bolliger MF, Ishihara H, Frei K, Bluethmann H, Gloor SM. Down-regulation of occludin expression in astrocytes by tumour necrosis factor (TNF) is mediated via TNF type-1 receptor and nuclear factor-kappaB activation. J Neurochem 2001e:78;155-62.

57. Tu J, Stoodley MA, Morgan MK, Storer KP. Ultrastructural characteristics of hemorrhagic, nonhemorrhagic, and recurrent cavernous malformations. J Neurosurg 2005e:103;903-9.

58. Fujimura M, Watanabe M, Shimizu H, Tominaga T. Expression of matrix metalloproteinases (MMPs) and tissue inhibitor of metalloproteinase (TIMP) in cerebral cavernous malformations: immunohistochemical analysis of MMP-2, -9 and TIMP-2. Acta Neurochir (Wien) 2007e:149;179-83; discussion 83.

59. Hou WK, Xian YX, Zhang L, Lai H, Hou XG, Xu YX, Yu T, Xu FY, Song J, Fu CL, Zhang WW, Chen L. Influence of blood glucose on the expression of glucose trans-porter proteins 1 and 3 in the brain of diabetic rats. Chin Med J (Engl) 2007e:120;1704-9.

60. Dejana E, Corada M, Lampugnani MG. Endothelial cell-to-cell junctions. FASEB J 1995e:9;910-8.

61. Birukova AA, Zebda N, Fu P, Poroyko V, Cokic I, Birukov KG. Association between adherens junctions and tight junctions via Rap1 promotes barrier protective effects of oxidized phospholipids. J Cell Physiol 2010e.

Formatted: German (Switzerland)

Formatted: Italian (Italy)

Figure Legends

FIGURE 1. Localization of the tight junction protein occludin (green) in CCM specimens: Confocal z-series projections of CCM#1, CCM#2 (A-B) and control samples c#2, c#4 (C-D). Occludin is distributed in a linear pattern along vessels of control tissues (C': cross sectional; D': longitudinal). Occludin is redistributed and shows decreased expression in ECs of CCMs (A': cross sectional; B': longitudinal). The endothelial cell marker protein PECAM-1 (CD31) is stained in red (A''-D''). DAPI (blue) is shown in A-D and merged images in A'''-D'''. Bars: 20 µm.

FIGURE 2. Distribution of TJP claudin-5 (green) and localization of EC-marker CD31 (red: A''-D'') in CCM specimens: CCM#2, CCM#3 (A-B) and controls: c#2, c#4 (C-D) by confocal microscopy. ~~Lik~~ ~~e occludin, claudin~~Claudin-5, same as occludin, is distributed linearly in vessels of control tissues (C': cross sectional; D': longitudinal). In CCM endothelial cells, claudin-5 expression is decreased (A' and B': cross sectional). DAPI (blue) is shown in A-D and merged images in A'''-D'''. Bars: 20 µm.

FIGURE 3. Confocal microscopy images of TJP ZO-1 (green) and CD31 (red) of CCMs (CCM#2, CCM#3) and ~~in~~ control specimens (c#1, c#4). ~~Like~~ As in control tissue section stainings for occludin and claudin-5, ZO-1 is distributed in a typical linear vessel pattern (C': cross sectional; D': longitudinal). In contrast, ZO-1 is significantly decreased (A'-B': cross sectional) in CCM samples. DAPI (blue) is mapped in A-D and merged images in A'''-D'''. Bars: 20µm.

~~**Fig4:** Confocal imaging of cryosections of CCM (CCM#1, CCM#6) and control tissues (c#1, c#5) immunostained for GLUT-1 (green) and CD31 (red). In control vessels, GLUT-1 is distributed uniformly (C': cross/longitudinal; D': longitudinal). However, the glucose transporter 1 is massively downregulated in CCM tissue samples (A': cross sectional; B': cross/longitudinal). DAPI (blue) is mapped in A-D and merged images in A''' D'''. Bars: 20µm.~~

FIGURE 4. Immunostaining for occludin (green) and collagen IV (red) on two CCM and NBT samples, respectively. Different phenotypes of occludin distribution are observed. Similar to control vessels, the linear pattern of occludin staining is preserved but thinned (A: longitudinal). To some extent, occludin is arranged in a punctate pattern along cell-cell contacts (B: longitudinal). At other

foci, vessels are completely unstained along the major length of their profile but show isolated, residual protein aggregates (C: cross sectional). Occludin is distributed in a linear pattern in microvessels of the adult human brain (cerebral cortex) (D and E). Basement membranes of capillaries are labeled by collagen IV-antibody (A-E). Nuclear staining with TO-PRO3 (blue) is shown in A-E. Bars: A, B and D, E 25 µm; C 10 µm.

FIGURE 5. Immunostaining for claudin-5 (green) and collagen IV (red) on two CCM specimens and NBT. In most instances, vessels appear negative for claudin-5. At some foci, claudin-5 is diffusely distributed within the tissue and not localized to intercellular contact sites (A: cross sectional). Few vessels show a punctate staining pattern (B: cross sectional). Decreased claudin-5 staining is seen along the EC cell contacts (C: cross sectional). Linear claudin-5 staining in capillaries of control NBT (D: longitudinal). Basement membranes of microvessels are labeled by collagen IV-antibody (A-D). Nuclear staining with TO-PRO3 (blue) is shown in A-C. Bars: A/D 30 µm; B/C 10 µm.

FIGURE 6. Confocal imaging of cryosections of CCM (CCM#1, CCM#6) and NBT (c#1, c#5) immunostained for GLUT-1 (green) and CD31 (red). In control vessels, GLUT-1 is distributed uniformly (C': cross/longitudinal; D': longitudinal). However, the glucose transporter 1 is massively downregulated in CCM tissue samples (A': cross sectional; B': cross/longitudinal). DAPI (blue) is mapped in A-D and merged images in A'''-D'''. Bars: 20µm.

FIGURE 7. Localization of fibronectin (green) and collagen VI as EC-marker (red: A''-B'') in CCM specimens: CCM#5 (A) and control: c#1 (B) by confocal microscopy. In vessels of the control tissue, fibronectin is distributed regularly (B': cross sectional). In CCM endothelial cells, fibronectin expression is impaired and irregular (A': cross sectional). DAPI (blue) is shown in A+B and merged images in A'''+B'''. Bars: 20 µm.

~~**Fig7:**~~**FIGURE 8.** Analysis of FI of occludin, claudin-5, ZO-1 and GLUT-1 stainings in cryosections of CCMs and control tissues. Experiments were done in triplicates. (A) MFI of each CCM and control specimen; (B) MFI (in %) of the seven normalized CCM specimens versus controls. Mean control

MFI was calculated as 100% (mean ± standard error of mean). Changes in MFI were calculated as highly significant for all proteins examined (students *t*-test, $p < 0.0001$, ****).

~~Fig8:~~**FIGURE 9.** Relative mRNA expression ~~(by microarray analysis)~~ of occludin, claudin-5, ZO-1 and GLUT-1 in CCM and NBT. ~~Mean value of relative mRNA levels of four EC-markers were calculated. Values for expression levels of named genes were consequently divided by the value of EC-markers. Calculation was done for each CCM (n=6) and STA (n=3) specimen.~~ Data is shown as mean values ± SEM of two individual experiments with eight samples in each group. Data were normalized against the EC-marker gene CD31. mRNA expression levels from NBT (n=8) are set to as 100% (mean ± standard error of the mean). Differences in mRNA concentrations were determined by the Mann-Whitney-Wilcoxon test with $p < 0.05$ being considered statistically significant.

Legends to supplementary figures

FIGURE S1. Confocal imaging of paraffin sections of CCM (CCM#1) and NBT (c#1) immunostained for occludin (green) and vWF (red). In control vessels, occludin is distributed in a linear pattern (C': cross sectional; D': longitudinal). However, occludin is massively downregulated in CCM tissue samples (A' and B': cross sectional). DAPI (blue) is mapped in A-D and merged images in A'''-D'''. Bars: 20µm.

FIGURE S2. Immunostaining for GLUT-1 (green) and vWF (red) in paraffin embedded CCM and NBT specimens (CCM#3; c#1). Decreased or absent GLUT-1 staining is seen in vessels of CCM tissue (A' and B': cross sectional). In capillaries of control NBT, GLUT-1 is distributed uniformly (C': cross sectional; D': longitudinal). ECs are labelled against the marker protein vWF (A''-D''). Nuclear staining with DAPI (blue) is shown in A-D. Bars: 20 µm.

Color Figure - Agree to Pay Publication Charges
Click here to download high resolution image

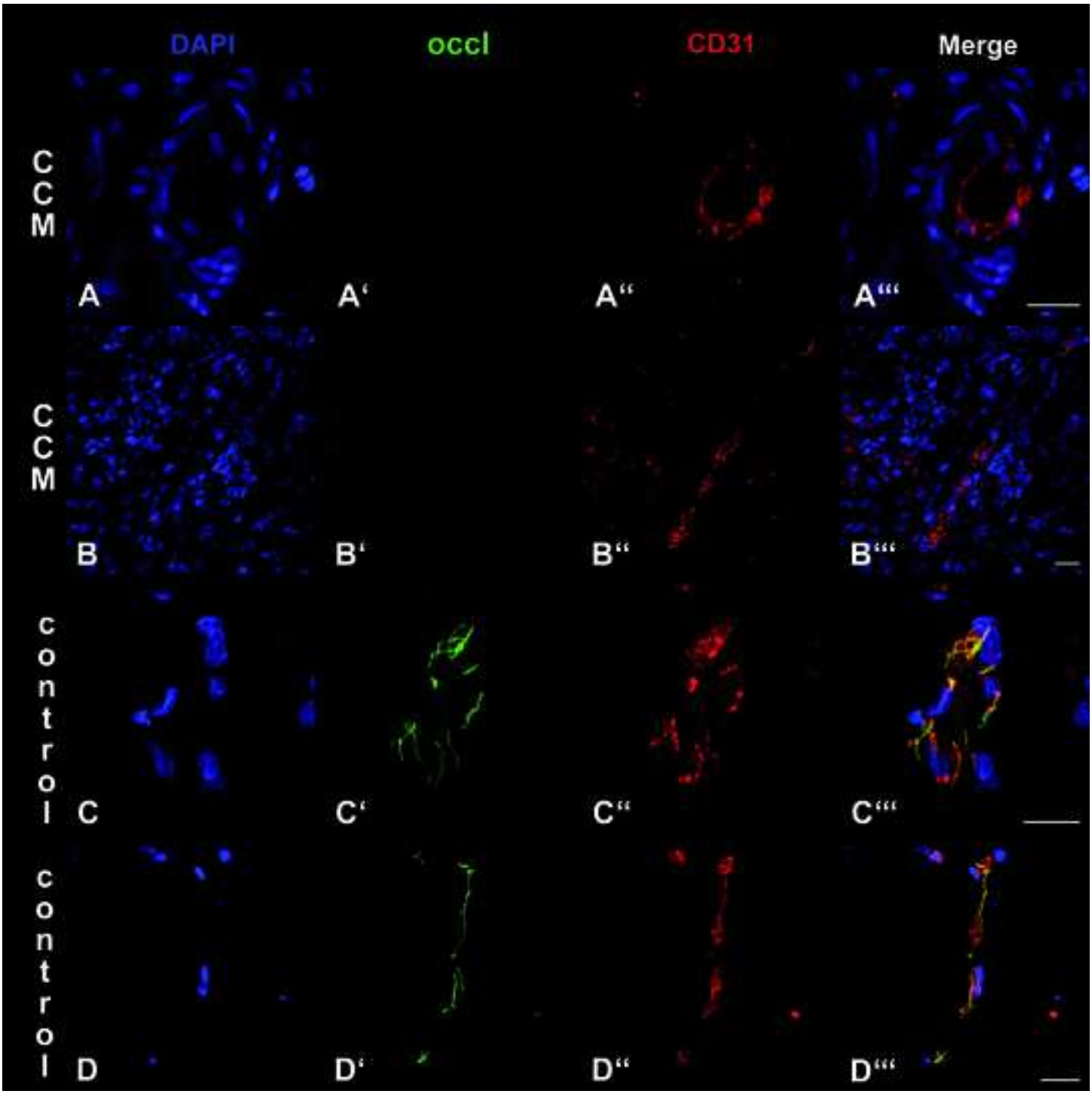

Color Figure - Agree to Pay Publication Charges
Click here to download high resolution image

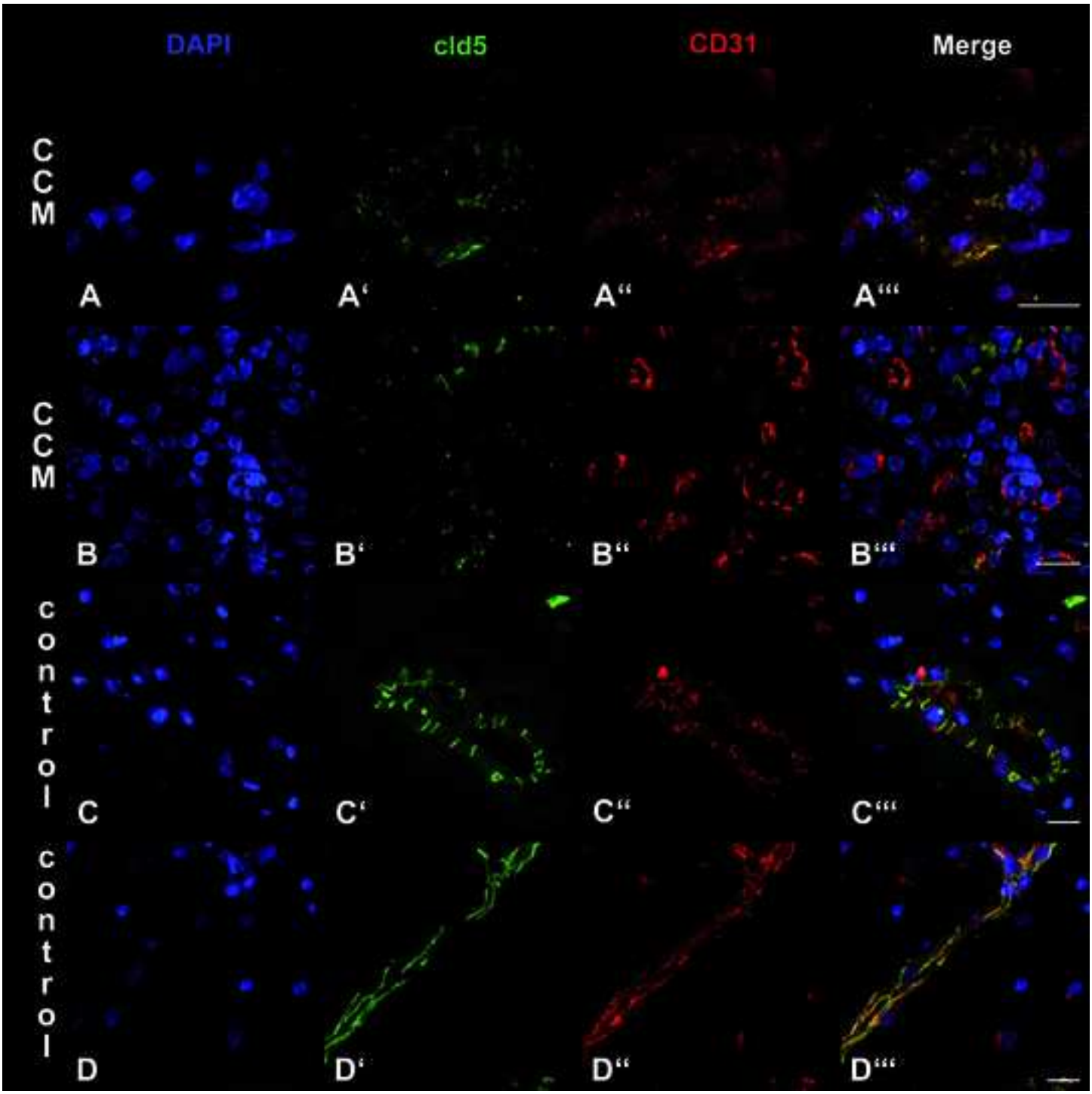

Color Figure - Agree to Pay Publication Charges
Click here to download high resolution image

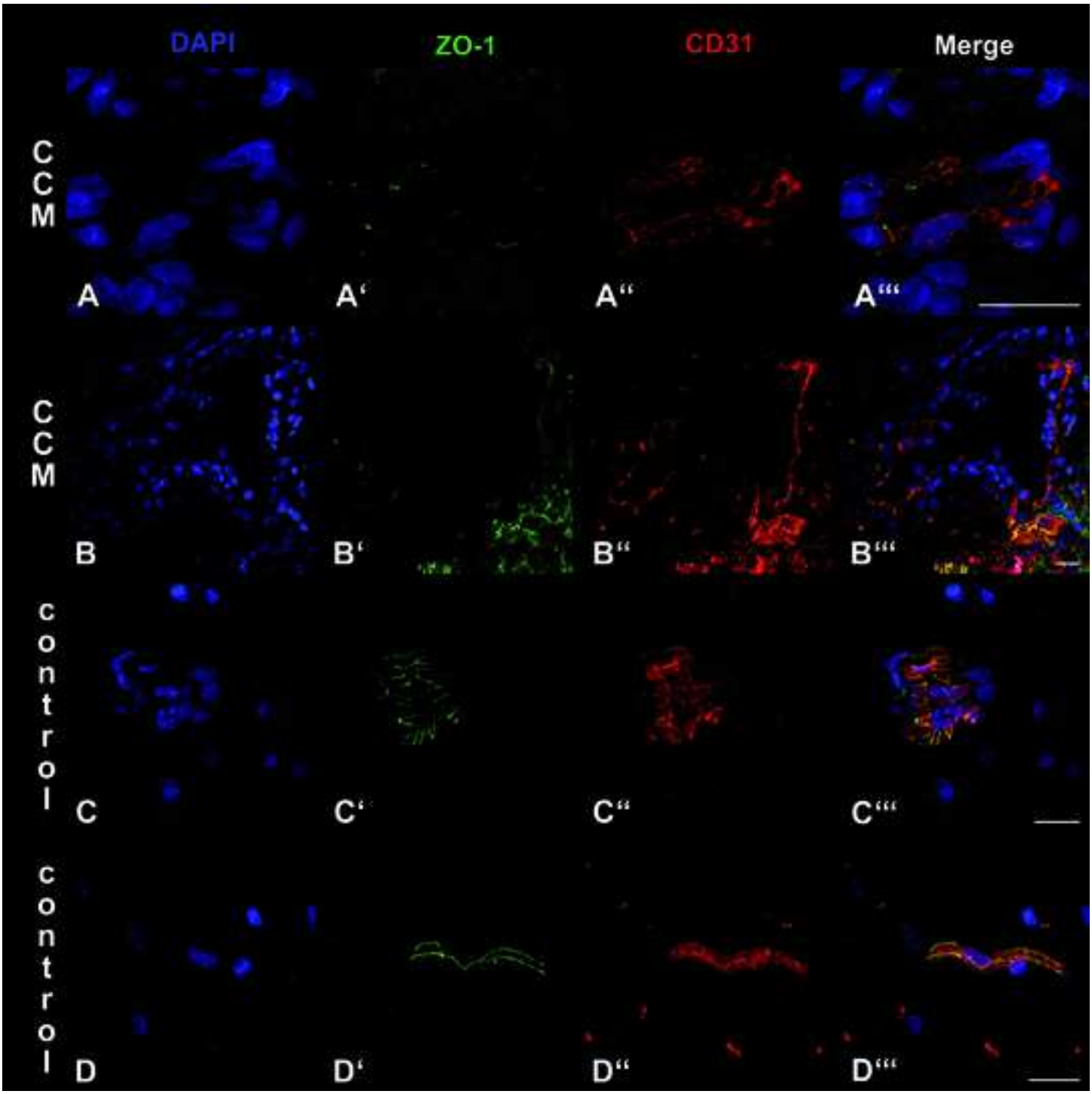

Color Figure - Agree to Pay Publication Charges
Click here to download high resolution image

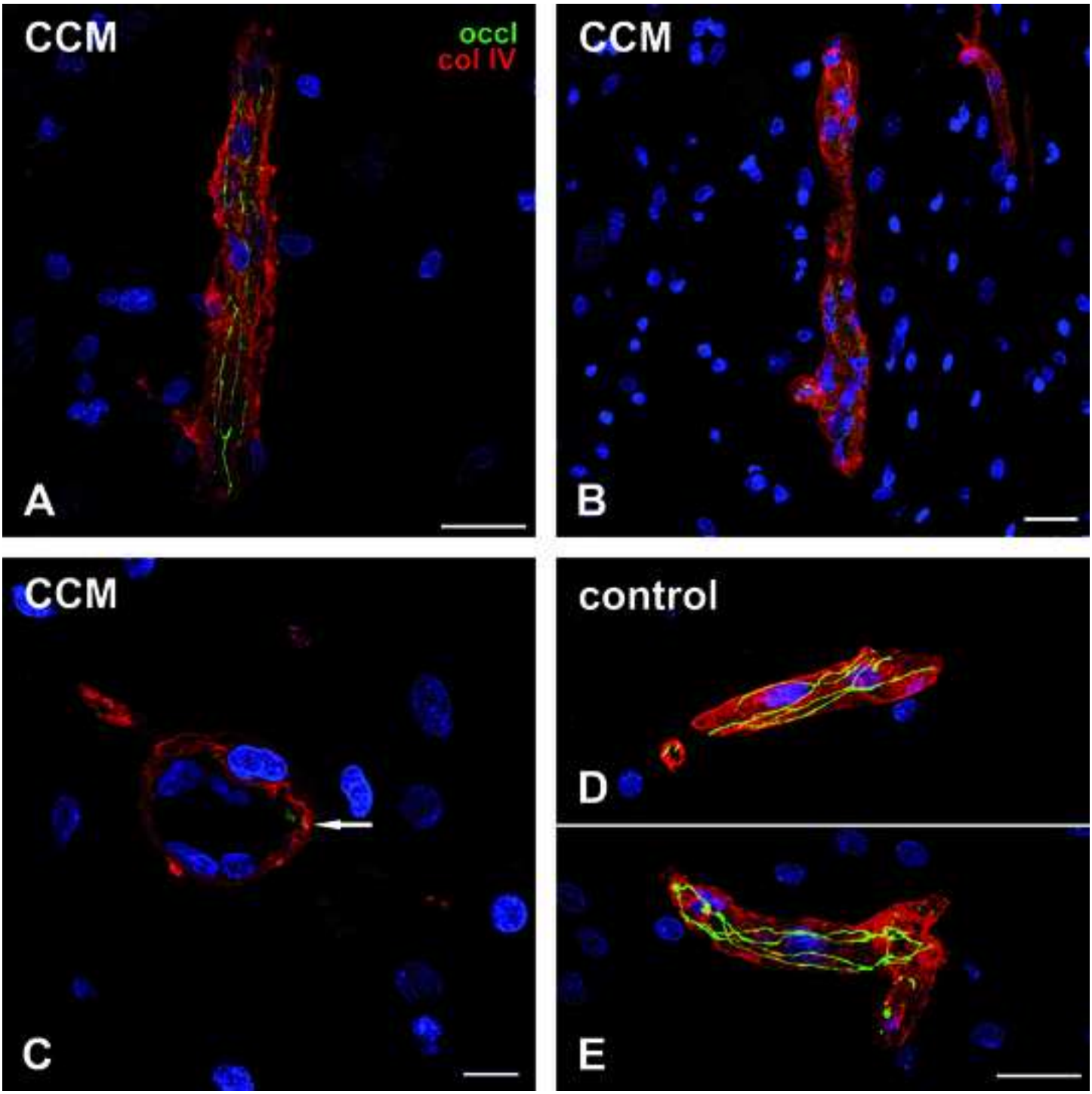

Color Figure - Agree to Pay Publication Charges
Click here to download high resolution image

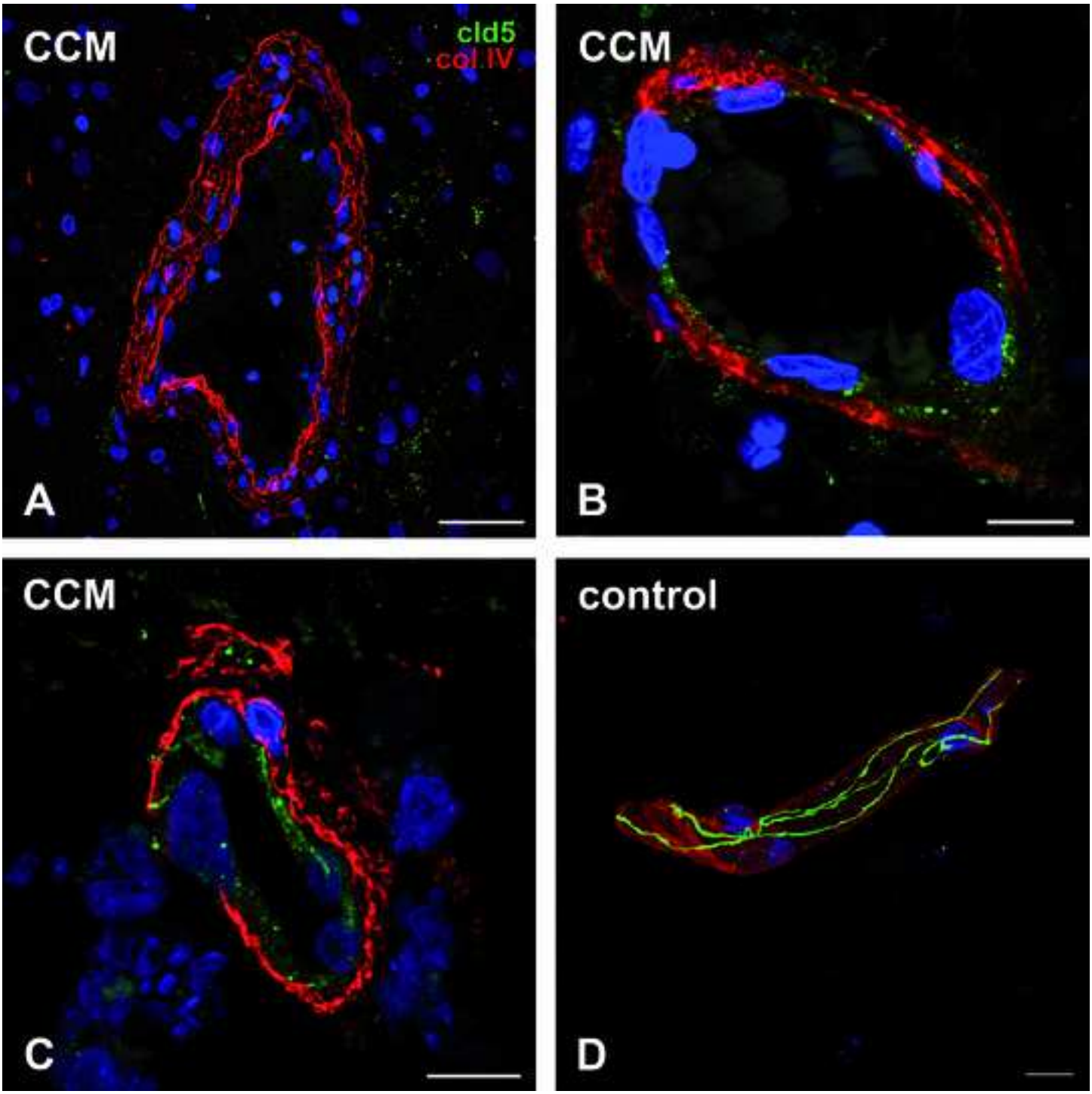

Color Figure - Agree to Pay Publication Charges
Click here to download high resolution image

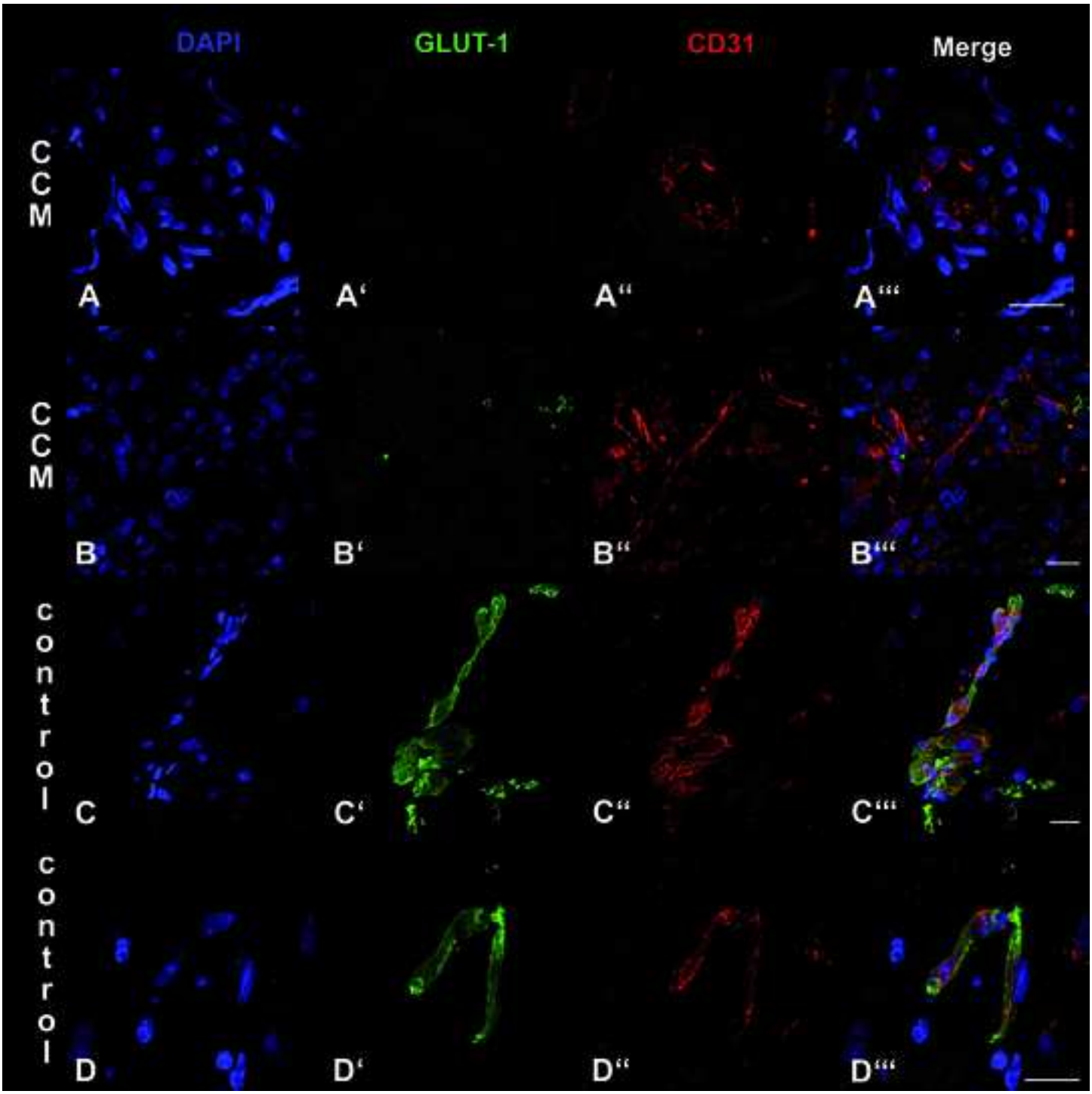

Color Figure - Agree to Pay Publication Charges
Click here to download high resolution image

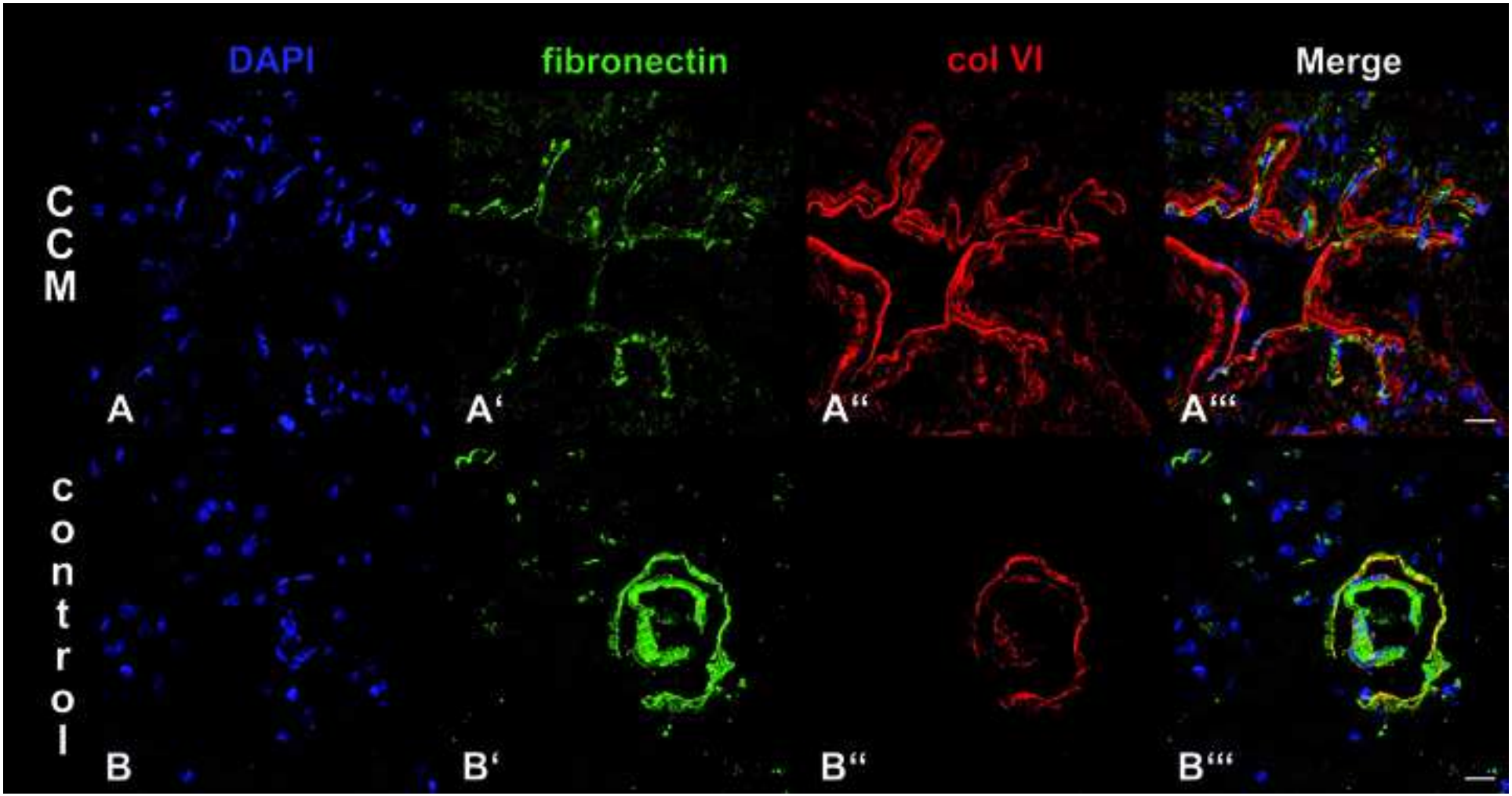

Color Figure - Agree to Pay Publication Charges
Click here to download high resolution image

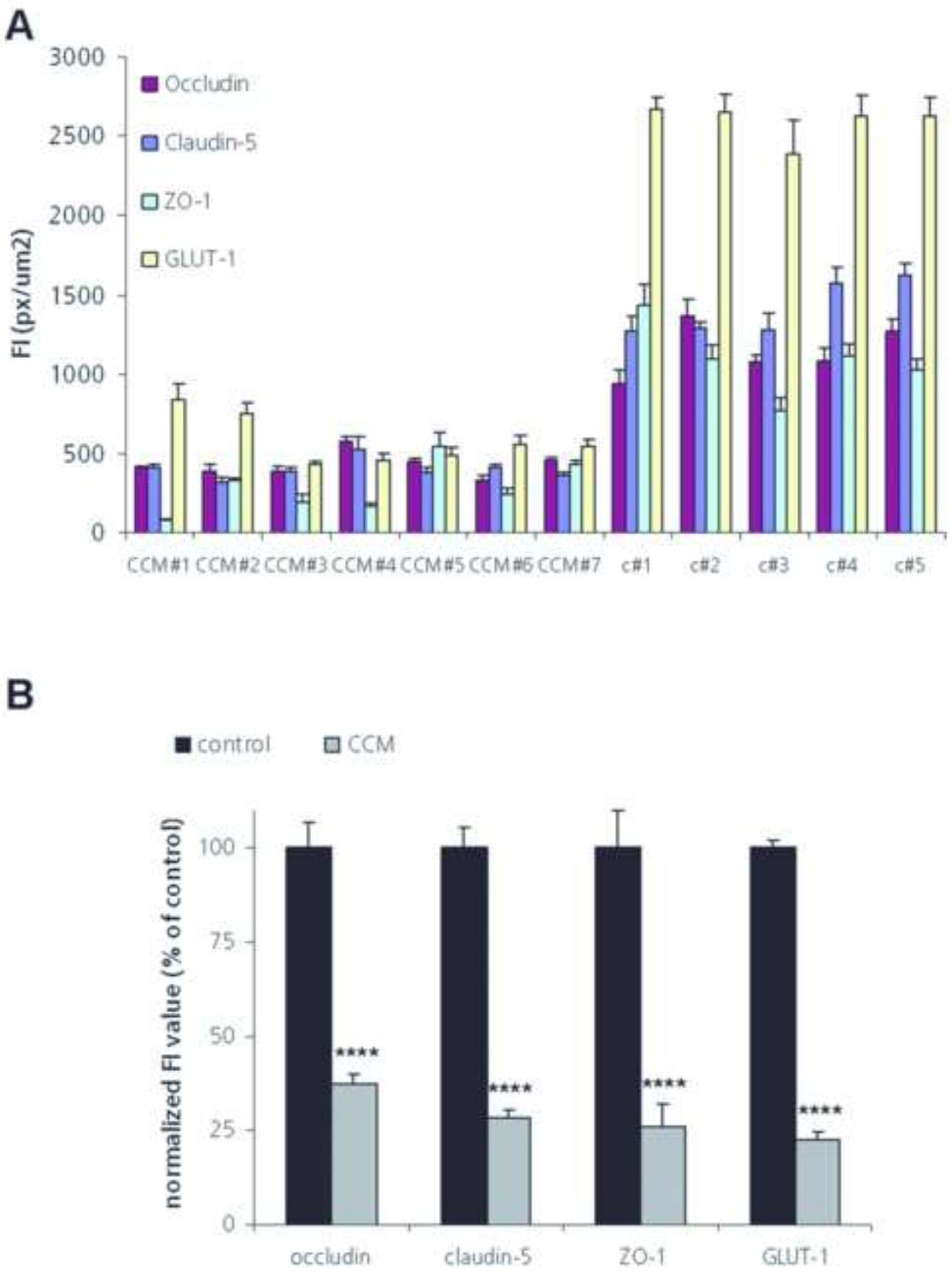

Figures Printed Black / White - No Publication Charges
Click here to download high resolution image

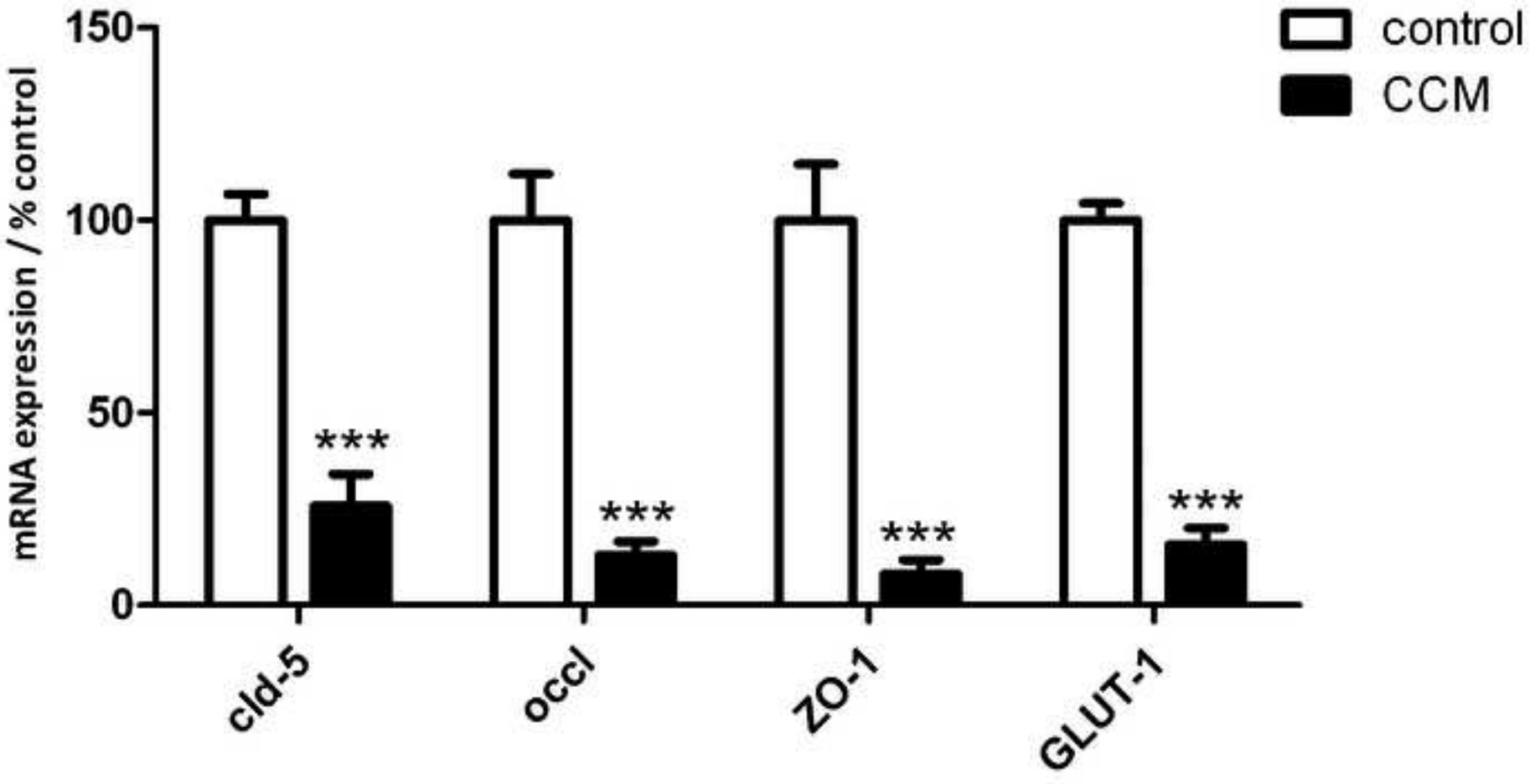

Supplemental Data File (.doc, .tif, pdf, etc.)

Click here to download Supplemental Data File (.doc, .tif, pdf, etc.): schneider_supplementary figure1.tif

Supplemental Data File (.doc, .tif, pdf, etc.)

Click here to download Supplemental Data File (.doc, .tif, pdf, etc.): schneider_supplementary figure2.tif

Table 1: Primer sequences for qRT-PCR

occludin forward	CACACAGGACGTGCCTTCAC
occludin reverse	GAGTATGCCATGGGACTGTCAA
claudin-5 forward	CTGCTGGTTCGCCAACATT
claudin-5 reverse	TGCGACACGGGCACAG
ZO-1 forward	CAGCCGGTCACGATCTCCT
ZO-1 reverse	TCCGGAGACTGCCATTGC
GLUT-1 forward	TGCTCATGGGCTTCTCGAA
GLUT-1 reverse	AAGCGGCCCAGGATCAG
CD31 forward	TCTCCCAGCCCAGGATTTC
CD31 reverse	TTCGATGGTCTGTCCTTTTATGAC
vWF forward	AGAAACGCTCCTTCTCGATTATTG
vWF reverse	TGTCAAAAAATTCCCCAAGATACA

Table 2: Clinical findings of enrolled patients in the study (40)

Patient baseline characteristics						Characteristics of CCM lesions			
patient no.	age/sex	ethnicity	clinical presentation	radiological findings	family history	lesion location	size (diameter in mm)	multiple lesions	DVA/associated
CCM#1	38M	caucasian	SH	RH	non	Rt. parietal	29	N	N
CCM#2	23F	caucasian	SH	RH	non	Rt. brachium pontis	10	Y	N
CCM#3	48F	caucasian	SH	NRH	yes	Lt. brachium pontis	12	Y	N
CCM#4	34F	caucasian	NH-FND	NRH	non	Lt. pedunculus cerebr	14	N	Y/Y
CCM#5	36F	caucasian	SH	RH	non	Lt. insular	9	N	Y/Y
CCM#6	6M	caucasian	SH	NRH	non	Rt. pons	23	N	N
CCM#7	14F	caucasian	SH	NRH	non	Rt. pons	20	N	N
CCM#8	35F	caucasian	NH-FND	NRH	non	Lt. pons	15	N	Y/Y
CCM#9	7 F	caucasian	NH-FND	NRH	non	Rt. subinsular	20	N	N
CCM#10	27 F	caucasian	SH	RH	non	Lt. pons	15	N	Y/Y
CCM#11	39M	caucasian	NH-FND	RH	non	Rt. occipital	20	N	N
CCM#12	47 F	caucasian	SH	NRH	non	Pons	17	N	Y/Y

M, male; F, female; SH, symptomatic hemorrhage; NH-FND, non-hemorrhagic focal neurological deficit; RH, recent hemorrhage; NRH, no recent hemorrhage; DVA, developmental venous anomaly; Y, yes; N, no.

***Copyright Transfer Form**

This piece of the submission is being sent via mail.